A&A 517, A93 (2010)
DOI: 10.1051/0004-6361/200912549

Astronomy & Astrophysics

On emission-line spectra obtained from evolutionary synthesis models

II. Scale-relations and the estimation of mass dependences

M. Villaverde[1], M. Cerviño[1], and V. Luridiana[2,3,1]

[1] Instituto de Astrofísica de Andalucía (CSIC), Glorieta de la Astronomía s/n, 18080 Granada, Spain
e-mail: [mva;mcs;vale]@iaa.es
[2] Instituto de Astrofísica de Canarias, C/ vía Lactea s/n, 38205 La Laguna, Spain
[3] Departamento de Astrofísica, Universidad de La Laguna (ULL), 38205 La Laguna, Tenerife, Spain

Received 20 May 2009 / Accepted 6 May 2010

ABSTRACT

Aims. In this paper we study the influence of the ionizing cluster mass on the emission line spectrum of H II regions in order to determine the influence of low mass clusters on the integrated emission line spectra of galaxies.
Methods. For this purpose, we present a grid of photoionization models that covers metallicities from $Z = 0.001$ to $Z = 0.040$, ages from 0.1 to 10 Ma (with a time step of 0.1 Ma), and cluster initial masses from 1 to 10^7 $M_\odot$. The stellar masses follow a Salpeter initial mass function (IMF) in an instantaneous burst mode of star formation. We obtain power-law scale-relations between emission-line luminosities and ionizing cluster masses from the grids and we evaluate the dependences on the ionizing cluster mass for some line luminosities, equivalent widths and line ratios.
Results. Power-law scale-relations are shown to be useful tools to obtain robust diagnostics, as examples: (a) Hα/Hβ ratio varies from the usually assumed value of 2.86, these variations imply the existence of a lower limit to the attainable precision in extinction estimations of $\Delta E(B-V) \sim 0.1$; (b) EW(Hβ) is a good age indicator with a small dependence on cluster mass, while EW([O III] 5007) shows a noteworthy mass dependence; (c) abundance estimations from R_{23} are practically unaffected by variations of the cluster mass; (d) estimations from S_{23} and η' would improve if the cluster mass dependences were considered; and (e) [O II] 3727/Hα is a good star formation rate indicator for ages older than ~4.5 Ma. We also show that the ionizing cluster mass dependence explains why empirical calibrations produce more reliable diagnostics of some emission lines than photoionization models grids. Finally, we show preliminary results about the contribution of low mass clusters ($M < 10^4$ $M_\odot$) to the integrated emission line spectra of galaxies, which can be as high as 80% for some relevant lines.

Key words. HII regions – galaxies: starburst – galaxies: star clusters

1. Introduction and motivation

The intrinsic properties of star forming regions are often inferred from observations of emission-line indicators. Examples of these indicators are the equivalent width of Hβ (EW(Hβ)) for age estimations, the radiation softness parameter η' (Vílchez & Pagel 1988) for cluster effective temperature ($T_{\rm eff}$) estimations, or the R_{23} (also called O_{23}) (Pagel et al. 1979) and S_{23} (Vílchez & Esteban 1996) parameters as abundances indicators. Some reviews that deal with these indicators have been written by Ferland (2003), Stasińska (2004) and Stasińska (2007).

These and other indicators are used in estimation-methods and/or classification methods, like the Baldwin et al. (1981) and Veilleux & Osterbrock (1987) diagnostic diagrams. These methods make use of only a handful of emission lines, more specifically, Hα, Hβ and some collisional lines of ions of O, N and S, so the understanding of the dependence of the intensities of such lines on the physical properties would allow us to calibrate the estimation methods.

When using theoretical methods for such indicator-calibration purposes, photoionization models and stellar population synthesis models prove to be very useful tools, as they allow the control of relevant physical parameters and return the possible emission line spectrum associated with such physical conditions. Nevertheless, one of the main issues that limits their power is the difficulty of establishing whether the solution found is unique for a given observation. One way to deal with such problem is building tailored models in which as many observational constraints as possible are assumed: an example of this strategy is offered by Luridiana et al. (1999); Luridiana & Peimbert (2001) and Luridiana et al. (2003), where models that simultaneously reproduce the intensity of several emission lines observed through different apertures are computed. A different approach is to compute grids or sequences of models. In this case fewer parameters are used but they span a larger range of values; this allow to apply the grids or sequences to diverse objects. Some examples can be found in the works of Huchra (1977), Olofsson (1989), García-Vargas & Díaz (1994), Stasińska & Izotov (2003) and Dopita et al. (2006b), among others.

One of the parameters that can be considered in the model grids for star forming regions is the ionizing cluster mass. Yet, in spite of being a fundamental physical property, little work has been done regarding the ionizing cluster mass. Examples can be

found in García-Vargas et al. (1995a,b), Stasińska & Leitherer (1996), Stasińska et al. (2001), and in a more indirect way in Dopita et al. (2006b), nevertheless the explicit dependence with the mass is not discussed in these works.

In this work we center our attention explicitly on the influence of the ionizing-cluster mass on the emission-line spectra. There are two motivations for this choice. The first one is the long term goal of investigating the accuracy of the modeling of the emission line spectra of ionizing clusters by means of evolutionary synthesis models, and the influence of sampling effects in the initial mass function (IMF) on the emission line spectrum (Cerviño et al. 2003, Paper I). In the first paper of the series we investigated when sampling effects in the stellar populations of the cluster cannot be neglected in the modelling of the emission line spectrum, and we showed that cluster masses must be larger than $10^3\ M_\odot$ to obtain realistic results for relevant emission lines, $10^3\ M_\odot$ being the cluster mass limit where a single star is as luminous as the whole cluster (that is, the *Lowest Luminosity Limit* (LLL), see also Cerviño & Luridiana 2004, for more details). Cerviño & Luridiana (2004) propose to use the mean values obtained from synthesis models in clusters at least 10 times larger than the LLL to minimize IMF sampling effects. In this second paper we aim to obtain a reference scale (calibrated with the cluster mass) that provide a mean reference value that allows to evaluate quantitatively the dispersion due to the IMF sampling. As it is known, and we will see below, the intensity of hydrogen recombination lines roughly scale with the number of ionizing photons, and hence with the number of massive stars and the mass of the cluster. However, a similar scale relation has not been established for the case of forbidden lines. In the last paper of this series, we will use these scale relations to evaluate the variance due to IMF sampling in the emission line spectrum as a function of the cluster mass.

The second motivation is to investigate the emission line spectrum of galaxies by the composition of different HII regions. In general, the emission lines spectrum of galaxies has been modeled by means of single photoionization models where all the stars are concentrated in a single point (whatever the stellar density of such hypothetic point) and with a single ionized gas nebula (Stasińska et al. 2001; Charlot & Longhetti 2001, as examples). Only few attempts have been done to consider an ensemble of clusters (Jamet & Morisset 2008) and to include an initial cluster mass function (ICMF) in the simulations (Dopita et al. 2006a). It can be claimed that the form of the ICMF[1] is such that each logarithmic bin of cluster mass contributes a similar amount to the total flux and massive clusters will therefore tend to wash out the stochastic effects of low-mass clusters (Dopita et al. 2006b). However, this statement implicitly assumes that the flux of *all relevant emission lines, including collisional ones*, scale linearly with the cluster mass. Checking the validity of such statement is the second objective of this paper.

To study these questions we have computed a grid of photoionization models with ionizing clusters of different masses. In this paper we do not consider sampling effects but the scale-relations of the emission line intensities with the ionizing cluster total mass. We have included in our study some extreme (unrealistic) cases of cluster masses (e.g. clusters with masses lower than $10^3\ M_\odot$, affected by sampling effects, or clusters with masses larger than $10^7\ M_\odot$, which are not consistent with the assumption of an instantaneous burst scenario). Such extremes allow us to explore the range where the scale relations are valid in a photoionization model, despite that they cannot represent real clusters, as well as to check if the emission line spectrum of a non-active galaxy can be modeled as a single nebula.

In the next section the properties of this grid of photoionization models are described and the differences with grids from other authors are discussed. In Sect. 3 the results of the models are analysed and the luminosity functions are computed. In Sects. 3.2.1 and 3.2.2 the reliability of these functions is checked comparing it with the results obtained directly from the models. The implications that arise from the analysis are discussed in Sect. 4, and finally the conclusions of this work are summarized in Sect. 5.

2. Modeling strategy: defining the grid

In the following we describe the input parameters assumed for the grid, and the differences with the grids elaborated by other authors.

2.1. Continuum shape and intensity

In this work we have used the spectral energy distributions (SEDs) computed with the evolutionary code by Cerviño et al. (2002a). All the computations assume an instantaneous burst of star formation and a Salpeter (1955) IMF slope in the mass range 2 to 120 $M_\odot$. We have adopted the evolutionary tracks with standard mass-loss rates by Schaller et al. (1992); Schaerer et al. (1993a,b); Charbonnel et al. (1993), and the following atmosphere models: Schaerer & de Koter (1997) CoStar for main-sequence hot stars more massive than 20 $M_\odot$, Schmutz et al. (1992) for WR stars, and Kurucz (1991) for the remaining stars. No X-ray emission due to the conversion of kinetic energy or the presence of young Supernova Remnants has been included. The models have been computed for the five metallicities available in the Geneva track dataset (Z = 0.001, 0.004, 0.008, 0.020 and 0.040) and cover the age range from 0.1 to 10 Ma with a time step of 0.1 Ma. The resulting SEDs have been used as an input to the photoionization code *Cloudy* version 08.00, last described by Ferland et al. (1998).

The continuum intensity has been defined in terms of the amount of photons able to ionize hydrogen, $Q(\mathrm{H}^0)$. We have used $Q(\mathrm{H}^0)$ values that correspond to amounts of gas transformed into stars at the onset of the burst ranging from 1 to $10^7\ M_\odot$. The mass step in the most relevant range (10^3–$10^6\ M_\odot$) is 0.5 dex while for lower masses the mass step is 1 dex. Obviously the 1 $M_\odot$ case is just an academic case, since the lower mass limit of the IMF is 2 $M_\odot$. Moreover, clusters with masses below $10^3\ M_\odot$ are also academic cases, since the (average) SED used would not be representative of real clusters (Cerviño et al. 2003; Cerviño & Valls-Gabaud 2003; Cerviño & Luridiana 2004, 2006). Whatever the case, the extension down to fictitious 1 $M_\odot$ clusters allows to explore the proportionality of the resulting emission line spectrum with the incident ionizing flux, independently of how "real" the incident flux is.

This strategy differs from the one by Dopita et al. (2000), who use the SED of a zero-age stellar cluster to build a grid where the metallicity and the ionization parameter of the model nebulae are varied. It is important to note that using a zero-age SED is roughly equivalent to using a single stellar atmosphere model with $T_{\rm eff}$ between 45 000 and 50 000 K (cf. Mas-Hesse & Kunth 1991; García-Vargas et al. 1995a), with the exact value depending on metallicity. One of the conclusions of these authors, specifically that HII regions can be modelled with

[1] Assuming both a power law with a slope of −2 (Lada & Lada 2003), or a log normal with $\sigma = 1.7$ and $M_0 = 100$ (Dopita et al. 2006b).

zero-age SEDs, contrasts with the philosophy underlying evolutionary synthesis models, which are in their essence *evolutionary*. Additionally, were the SED of observed HII regions described by synthesis models at zero-age, then all observed HII regions should have similar Hβ equivalent widths (with values around 500 Å), which is clearly in contradiction with the observations. The fact that their grid reproduce the observed trends in some diagnostic diagrams is a nice example of the non-uniqueness of the possible physical conditions that produce a given emission line spectrum.

A strategy more similar to ours is the one by (García-Vargas et al. 1995a,b), who present their results in terms of ages, metallicity and initial amount of gas transformed into stars. Our modelling differs from theirs in (a) the metal mixture, especially for what concerns the N/O ratio, which in our grid varies with the metallicity, and (b) the geometry, which is spherical in our case and plane-parallel geometry in García-Vargas et al. (1995a).

Our grid is similar in approach to the one by Stasińska & Leitherer (1996) and Stasińska et al. (2001). Differences are in this case the metal mixture, and the higher resolution in age and cluster size in our grid with respect to theirs.

Finally, Dopita et al. (2006b) used for the grid a parameterization on metallicity, age and on a parameter that depends both on the ionizing cluster mass and on the pressure in the interstellar medium (ISM). In this sense the cluster mass is considered but its effects are mixed with the ones of the pressure. There are also differences in the metal mixture, in the age covering, which in our work is larger and has higher resolution, and in the covering factor, which in their work varies with the age.

2.2. The chemical composition mesh

In this work we assumed a dust-free nebula and the solar composition listed in Hazy (Ferland 2008, Table 14), which corresponds to the abundances by Grevesse & Anders (1989) with the extensions by Grevesse & Noels (1993) except for C, N, O and He. The solar oxygen abundance has been set to O/H = 4.91×10^{-4}, following Allende Prieto et al. (2001). The solar C/O ratio has been set to 0.5 (Allende Prieto et al. 2002), yielding a solar C abundance of 2.45×10^{-4}. For metallicities other than solar, the abundances have been linearly scaled with Z except for He and N. For the He abundance, we have used the following relation:

$$\frac{\mathrm{He}}{\mathrm{H}} = 0.0786 + 18.4\left(\frac{\mathrm{O}}{\mathrm{H}}\right), \quad (1)$$

which has been obtained from the value of the primordial helium abundance obtained by Luridiana et al. (2003), $Y_\mathrm{p} = 0.2391$, and the slope of the He vs. O relationship quoted by Peimbert et al. (2000), $\Delta Y/\Delta \mathrm{O} = 3.5$. Dopita et al. (2006b) assume for the He abundance a steeper relation given by:

$$\frac{\mathrm{He}}{\mathrm{H}} = 0.0737 + 52.5\left(\frac{\mathrm{O}}{\mathrm{H}}\right). \quad (2)$$

In the case of nitrogen, we have assumed the N/O ratio given by:

$$\log\left(\frac{\mathrm{N}}{\mathrm{O}}\right) = -1.5 \quad \text{for } \log\left(\frac{\mathrm{O}}{\mathrm{H}}\right) < -4.$$
$$= 1.1\log\left(\frac{\mathrm{O}}{\mathrm{H}}\right) + 2.9 \quad \text{for } \log\left(\frac{\mathrm{O}}{\mathrm{H}}\right) > -4.$$

The relation has been obtained by a fit by eye of the data presented in Pilyugin et al. (2003). It should be noted that, as shown by Pilyugin et al. (2003), an exact N/O ratio does not exist, since its value changes from system to system even for a fixed metallicity. This dispersion could arise naturally if the chemical evolution of a galaxy were driven by small star forming regions, so that the sampling effects of the IMF in the chemical evolution become relevant (White & Audouze 1983; Wilmes & Koeppen 1995; Cerviño & Mollá 2002; Carigi & Hernández 2008). Given this situation, we think it is more meaningful to fit the results by eye rather than using a formal method.

Table 1. Values of O/H implicit in the evolutionary tracks, in Stasińska et al. (2001) grid and in this work for a given Z.

Z	O/H (tracks)	Stasińska et al. (2001)	This work
0.0004	–	1.70×10^{-5}	–
0.001	4.39×10^{-5}	–	2.46×10^{-5}
0.004	1.77×10^{-4}	1.70×10^{-4}	9.82×10^{-5}
0.008	3.64×10^{-4}	3.40×10^{-4}	1.96×10^{-4}
0.020	9.75×10^{-4}	8.51×10^{-4}	4.91×10^{-4}
0.040	2.12×10^{-3}	1.70×10^{-3}	9.82×10^{-4}

We have also performed a consistency check on the assumed abundances of the stellar tracks. As explained in the corresponding papers (Schaller et al. 1992; Schaerer et al. 1993a,b; Charbonnel et al. 1993), the tracks assume a helium content by mass given by:

$$Y = = Y_\mathrm{p} + \frac{\Delta Y}{\Delta Z}Z, \quad (3)$$

with $Y_\mathrm{p} = 0.24$ and $\Delta Y/\Delta Z = 3$ for all metallicities except for the case $Z = 0.040$ (Schaerer et al. 1993a, twice solar) where $\Delta Y/\Delta Z$ takes a value of 2.5. Additionally, the relative ratios of heavy elements follow the ones obtained by the Anders & Grevesse (1989) solar mixture, somewhat different from the values by Grevesse & Anders (1989) quoted before, for all the metallicities. The absolute values have been scaled with Z except for $Z = 0.004$ (Charbonnel et al. 1993) and $Z = 0.040$ (Schaerer et al. 1993a) where Grevesse (1991)[2] has been used. Under this assumption, a N/O ratio of 0.15 is assumed for all the metallicities except for $Z = 0.004$ and $Z = 0.040$, where it is 0.13. This is clearly inconsistent with the mixture we assume in the nebular gas, but, since we are not able to quantify the influence of a change of the N/O ratio on stellar evolution, and we prefer to adopt a nebular metal mixture more consistent with the observational data, there is no solution other than maintaining the inconsistency and hoping that it only produces minor effects.

Finally, we have obtained the oxygen abundance from the different set of tracks. The resulting O/H values for each metallicity, Z, are summarized in Table 1, where we also show the gas O/H and Z values assumed in Stasińska et al. (2001) for comparison.

Since there is no feasible way of solving the inconsistency between the abundances of the evolutionary tracks and those adopted for the gas, present in our and similar works, we limit to call the attention to it and present our model grid in terms of Z, without expressing the metallicity as a function of the solar value. It should be kept in mind that a direct comparison with other works must be done with extreme caution.

[2] The reference paper cites Grevesse et al. (1991) instead of this one.

2.3. Density, geometry, filling factor and covering factors

The assumptions on the electronic density, the geometry, the filling factor and the covering factor define the properties of the model nebulae. For the case of the density and geometry we have assumed rather conservative values: a hydrogen constant density of 100 cm^{-3} distributed homogeneously over an expanding spherical geometry in an ionization bounded configuration. The assumed density of 100 cm^{-3} is typical for H II regions and it is lower than the critical densities of the species used in this work. The internal radius of the cloud, R_{in}, has been fixed for all the models to 2 pc ($\log R$(cm) = 18.790426).

The covering factor $\Omega/4\pi$ is the fraction of the solid angle around the ionization source covered by the gas nebula. There is a large amount of observational evidence (see e.g. Beckman et al. 2000; Zurita et al. 2002; Castellanos et al. 2002; Iglesias-Páramo & Muñoz-Tuñón 2002, among others) that a substantial fraction of the ionizing photons escape from the ionized nebulae. This finding may indicate either that the covering factor is smaller than one, or that the nebula is density bounded (or a mixture of both situations). Although the predictions of photoionization models differ in the two situations (see, e.g. Luridiana et al. 2003, for a full discussion), we have chosen to model the escape of ionizing photons adopting a covering factor and assuming the nebula ionization bounded, rather than assuming it density bounded. This choice has been motivated by simplicity considerations, since it offers the advantage of preserving the proportionality between the number of ionizing photons and the intensity of Balmer lines, in contrast to what happens in density bounded nebulae. This means that we can test L(Hβ) estimations by synthesis models based on Q(H^0). In this work we have assumed a covering factor equal to 1, although estimated values of the covering factor range between 0.2 and 0.8 (Zurita et al. 2002). Again, our choice is based on simplicity considerations, since our objective is to obtain the shape of the luminosity functions of the emission lines intensities but not to calibrate it.

For each age, metallicity and mass, the photoionization model has been computed until a minimum electron temperature has been reached. This minimum electron temperature is 4000 K for Z = 0.001, 0.004 and 0.008 and 200 K for Z = 0.020 and Z = 0.040. Once a solution has been found, it has been used as input for another iteration, and so on, until a stable solution has been found.

Additionally, we have obtained the continuum flux resulting from Cloudy, obtained directly with the `punch continuum` command. However, this continuum includes the luminosity of the resulting emission lines. To exclude the emission line contribution, we have obtained it using the `punch outward` continuum command and then subtract it from the continuum flux (see Ferland 2008, for more details on the use of this command and the `punch continuum` one). The resulting continuum has been used later to obtain the equivalent widths of the corresponding emission lines.

We want to note that the choices made here, especially those concerning the geometry, density, filling factor and covering factors are merely convenient choices: we are not suggesting that all HII regions can be modelled with this set of parameters. We are interested here only in obtaining a rough estimation of the relation of intensity of relevant emission lines with the stellar cluster mass and how these dependencies vary from line to line. This goal is the driver in our choice of the grid which drastically differs from how other authors define their grids, since they address a different problem from the one discussed here.

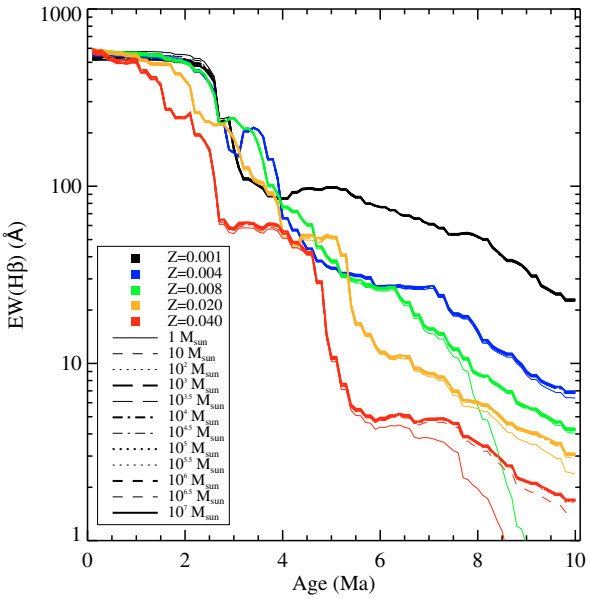

Fig. 1. Hβ equivalent width versus age. Grey scale colors represent metallicities. Thin solid line: 1 $M_\odot$. Thin dashed line: 10 $M_\odot$. Thin dotted line: 100 $M_\odot$. Thin long-dashed line: 10^3 $M_\odot$. Thick dash-dot line: 10^4 $M_\odot$. Thick dotted line: 10^5 $M_\odot$. Thick dashed line: 10^6 $M_\odot$. Thick solid line: 10^7 $M_\odot$.

3. Results of the grid models

In this section we analize the results from the models. First we center our attention on the two hydrogen recombination lines Hα and Hβ, specifically on their use for age and extinction estimations. Next we derive mass-luminosity scale-relations from the models and apply the same method to some relevant collisional lines. Finally we check the scale-relations results with the ones obtained directly from models.

3.1. Hydrogen recombination lines

3.1.1. Hβ equivalent width

The resulting EW(Hβ) from the grid is shown in Fig. 1. The plot shows the results for the complete grid (including all the assumed cluster masses). Different line types account for cluster masses while grey scale colors represent metallicities. For a given metallicity, the curves at different masses are similar with just slight differences that depend on the ionizing cluster mass. Excluding the 1 $M_\odot$ cases, these differences are always less than 0.1 dex. The 1 $M_\odot$ cases diverge from the rest of models at old ages because the computation goes deeper into neutral gas and the continuum at Hβ wavelenght increases.

As a safety check to the resulting EW(Hβ) from synthesis models computations, we have compared the ratio of the Hβ luminosity with the number of hydrogen ionizing photons, Q(H^0). Synthesis models assume a putative constant value around L(Hβ) = $4.8 \times 10^{-13}(\Omega/4\pi)Q$(H^0) (e.g. Cerviño & Mas-Hesse 1994; Leitherer & Heckman 1995) for T_e = 10^4 K, n_e = 100 cm^{-3} and He/H = 0.1. Figure 2 shows that the resulting conversion value for $M > 10^3$ $M_\odot$ only varies ~20% during the considered ages.

Summing up, EW(Hβ) is a "good enough" indicator of the age of an H II region (Copetti et al. 1986) once the covering factor is known. EW(Hβ) depends mainly on the metallicity (Cerviño & Mas-Hesse 1994) and age of the cluster with almost

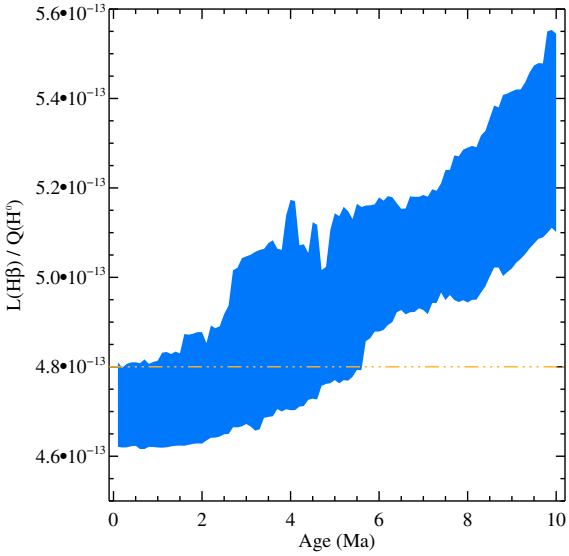

Fig. 2. Ratio of the Hβ luminosity to the number of hydrogen ionizing photons, $Q(H^0)$, versus age for models with $M \geq 10^3\ M_\odot$. The shaded zone corresponds to the range of values of the ratio. Dash-dot-dot line: value assumed by synthesis models.

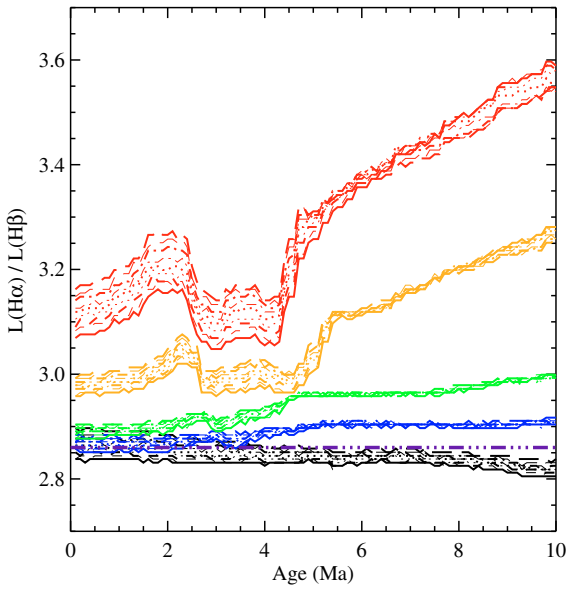

Fig. 3. Hα/Hβ ratio versus age. Dash-dot-dot line: normally assumed value. Rest of symbols as in Fig. 1.

no variations due to the size of the cluster, if sampling effects are not considered (but see Cerviño et al. 2000, 2002b).

3.1.2. Hα, Hβ and extinction

More interesting is the behaviour of the Hα/Hβ ratio, used commonly as an extinction index, and for which a constant ratio of 2.86 is normally assumed. Figure 3 shows such ratio, obtained for models with $M \geq 10^3\ M_\odot$, the line types have the same meaning as in Fig. 1. The ratio computed for case B and $T_e = 10^4$ K is also shown for comparison. The figure demonstrates that in fact such an assumption is incorrect. The largest discrepancies between the results of the models and the value normally assumed occur generally for $Z = 0.040$. Nevertheless, the largest ones correspond to models with $Z = 0.008$, 1 $M_\odot$ (not shown in the figure) and ages around 10 Ma, which are ~50% greater than the usual assumed value and lead to $E(B-V) = 0.36$. For that cluster mass the mean spectrum obtained by synthesis models is just an academic result, as we pointed out before. Considering only the models with $M \geq 10^3\ M_\odot$ a maximum discrepancy of 25.8% with respect to the ratio normally assumed is found for models with $Z = 0.04$, 10 Ma, and masses larger than $10^6\ M_\odot$. However, this only sets an upper limit to the bias since at such ages the H II region are so faint that they are not detected. Considering lower and more relevant ages (0.1–6 Ma), differences near 18% are found for $Z = 0.04$ and masses $10^{3.5}$ and $10^4\ M_\odot$ at 6 Ma. If we also exclude the highest metallicity models, differences near 9% are found for $Z = 0.02$, $M \geq 4.5\ M_\odot$ at ages near 6 Ma.

The use of an incorrect Hα/Hβ ratio leads to an incorrect extinction estimation which affects the line intensities inferred. For example, a difference of 9% with respect to the normally assumed ratio leads to a spurious $E(B-V) = 0.08$. Although this value is small, this exercise shows that $E(B-V)$ estimations from the emission line analysis (without the use of tailored models) suffer from intrinsic uncertainties which may be as large as 0.1. This effect is independent of the extinction due to the H II region dust content. If dust effects were taken in account, then the scatter in the Hα/Hβ ratio would be different: bigger HII regions would have a larger amount of dust, the dependence with the geometry would be stronger and a tailored analysis would be needed.

3.1.3. Scale-relations

In order to study the variation of the intensities of the emission lines considered in this work, we made ordinary least square linear regressions of the logarithm of the line intensities versus the logarithm of the cluster mass for each line, metallicity and age. The linear fits provide us scale-relations between the line intensities and the cluster mass of the form

$$\log(L) = \alpha + \beta \log(M), \tag{4}$$

or equivalently

$$L = A \times M^\beta, \tag{5}$$

where $A = 10^\alpha$. These scale-relations, as said above, have been built to obtain a first estimation of the behaviour of the emission lines with the mass of the cluster. Due to the assumptions made in the models and the simplicity of the description with power-laws, we strongly discourage from using this method when fine results are sought. Let us stress again that our goal is just to obtain an approximate quantitative representation of the H II region luminosity function.

The regressions have been computed only with models with $M \geq 10^3\ M_\odot$. This condition to the cluster-mass agrees with the minimum cluster mass obtained by Cerviño et al. (2003) for a reliable (although affected by sampling effects) description of the ionizing continuum by the mean ionizing continuum obtained in synthesis models. Regressions with models in all the mass range, including the purely academic case of clusters less massive than $10^3\ M_\odot$, have also been computed but they have been discarded, because the agreement in diagnostic diagrams between regressions and models in the high mass range is worse than when only models with $M \geq 10^3\ M_\odot$ are used (see Sect. 3.2.1).

We have also studied an a posteriori additional constraint on the observability of emission lines. This constraint has been parameterized in terms of a distinction between lines with

EW smaller and larger than 1 Å respectively. Of course, this is an optimistic value: if older stellar populations were present, the continuum level would be higher and the resulting *EW*s lower. However, we assume just a single stellar population in an instantaneous burst mode of star formation in our modeling. The effects of these additional populations on the continuum level and *EW*s measurements can be modeled through the use of a different star formation history, which goes beyond the scope of this paper.

The *EW* computations have been carried out using the line luminosity and the continuum luminosity as computed by Cloudy, which takes into account the two contributions to the continuum luminosity (stellar and nebular continua). We have obtained continuum scale relations using Eq. (4). As expected, the continuum luminosity (including the nebular contribution) scales linearly with the cluster mass, although there is a small dispersion when the continuum obtained from the scale relations is compared with the continuum from particular models (around 7%, compatible with the scatter in the hydrogen recombination lines shown previously). We have computed the EW of the emission line using the scale relations following:

$$EW = \frac{A_{\rm line} \times M^{\beta}}{A_{\rm cont} \times M} = \frac{A_{\rm line}}{A_{\rm cont}} \times M^{\beta-1}, \quad (6)$$

where $A_{\rm line}$, following Eq. (5), is the luminosity of the line when the cluster mass is 1 $M_{\odot}$, obtained from the extrapolation of the power law down to this value. Analogously, $A_{\rm cont}$ is the luminosity of the continuum when the cluster mass is 1 $M_{\odot}$. Since we are interested in the relation of the luminosities with the cluster mass, we center our attention on the slopes of the scale-relations. However, the *EW* obtained from the scale-relations are more dependent on the geometrical assumptions (inner radius, covering and filling factors) than the scale-relations slopes themselves, due to the large dependences of $A_{\rm line}$ and $A_{\rm cont}$ on the geometry. So, we will use this constraint on *EW* as a self-consistency check by comparing the results from models that fulfill $EW \geq 1$ with scale-relations results with *EW* estimations obtained from the scale-relations themselves. The values of the normalized luminosities will be shown in a posterior work when a proper ICMF and star formation history will be included for models of non-active emission line galaxies.

In Fig. 4 the slopes, the luminosity normalized to the total mass and the correlation factor (plotted as $1 - r$) as a function of the age obtained for Hβ line are shown. The slopes for Hβ intensity are practically constant and with a value almost equal to one. This behaviour is expected for hydrogen recombination lines (the Hα intensity shows similar results) because their intensity is practically proportional to the $Q(H^0)$ of the ionizing cluster, which is directly related with the cluster mass. This is coherent with the small range of the $L(H\beta)/Q(H^0)$ ratio shown in Fig. 2 for each age. Also, $1 - r \approx 0$ accounts for this proportionality.

Lines that have power-laws with $\beta \approx 1$ are particularly interesting because, as we have said, they vary linearly with the cluster mass, or equivalently with $Q(H^0)$, just as the continuum produced by the stellar cluster. In general, the use of line ratios with lines that have similar β values provide indices that are independent on the cluster mass, and so, such indices can be calibrated with observations of clusters without the need to worry about the cluster size (if IMF sampling effects are not taken into account). This is the case of $EW(H\beta)$, as can be seen in Fig. 1, because the intensity of the continuum is proportional to the cluster mass.

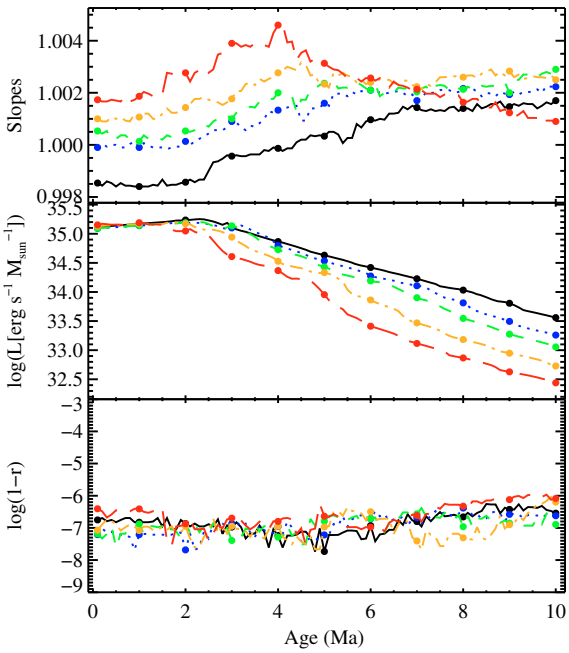

Fig. 4. *From top to bottom*: slopes, $\log(L[\mathrm{erg\,s^{-1}}\ M_{\odot}^{-1}])$ and correlation coefficient of linear regression of $\log(L(H\beta))$ versus $\log(M)$. Grey scale colors indicate metallicities as in Fig. 1. Dots indicate models with age equal to 0.1, 1, 2, 3, ... Ma.

3.2. Collisional lines

Following the same method described before we have obtained scale-relations for some relevant collisional lines. In Fig. 5 the slopes for [O II] λ 3727 Å, [O III] λ 5007 Å, [N II] λ 6584 Å, [S II] λ 6716 Å, and [S III] λ 9069 Å are shown. The grey scale colors of the lines have the same meaning as in Fig. 1. We have represented with dotted lines the ages where the scale relations computed through Eq. (6) do not produce $EW \geq 1$ Å for all masses in the 10^3–10^6 $M_{\odot}$ mass range (we have excluded the 10^7 $M_{\odot}$ case, since it is a purely academic case with no implications for observations). For these emission lines $r > 0.98$ in all the age range, therefore within our models the logarithm of the intensity of the emission lines is, to a good approximation, linear with the logarithm of the cluster mass.

The slopes of [O II] λ 3727 Å, [N II] λ 6584 Å, and [S III] λ 9069 Å have a similar behaviour. In the three cases, there are two regimes, a young one with slopes around 0.7–0.8, and an a older one with slopes around 1 (excluding the $Z = 0.04$ models). The transition between the two regimes happens in the age range 4–5.5 Ma and it is due to a softening of the ionizing continua in such age range. Comparing with the evolution of the cluster $T_{\rm eff}$, defined as in Mas-Hesse & Kunth (1991), the change in the slope is associated with a cluster $T_{\rm eff} \sim 3.5 \times 10^4$ K following the results from Cerviño & Mas-Hesse (1994) and Cerviño et al. (2002b)[3]. Such cluster $T_{\rm eff}$ is not due to the predominance of a specific type of star but to a mix of different types of stars.

Since the different values of the slopes indicate different dependences with the mass, and taking into account that the continuum is proportional to the cluster mass, it is straightforward that the equivalent widths also present different dependences with the mass. This can be seen in Fig. 6a in which *EW*([O II] 3727) is shown for $M \geq 10^3$ $M_{\odot}$ and all the metallicities. There is a clear dependence of *EW*([O II] λ 3727) with the mass for young ages

[3] http://www.laeff.inta.es/users/mcs/SED/index.html

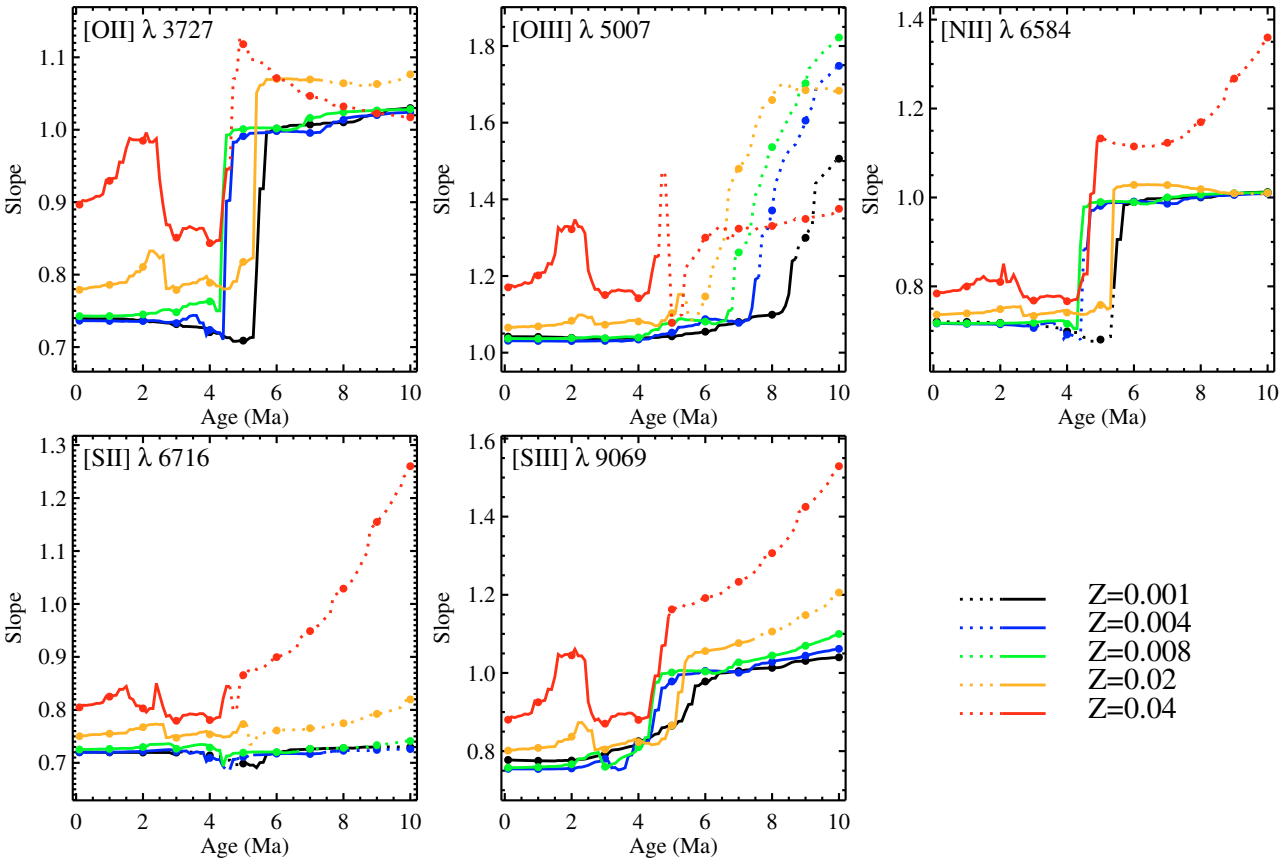

Fig. 5. Slopes of the scale-relations for some collisional lines. In the plot, the dotted section of the lines represents the ages where the $EW \geq 1$ Å is not fulfilled for all masses in the 10^3-10^6 $M_\odot$ mass range. Symbols as in Fig. 1.

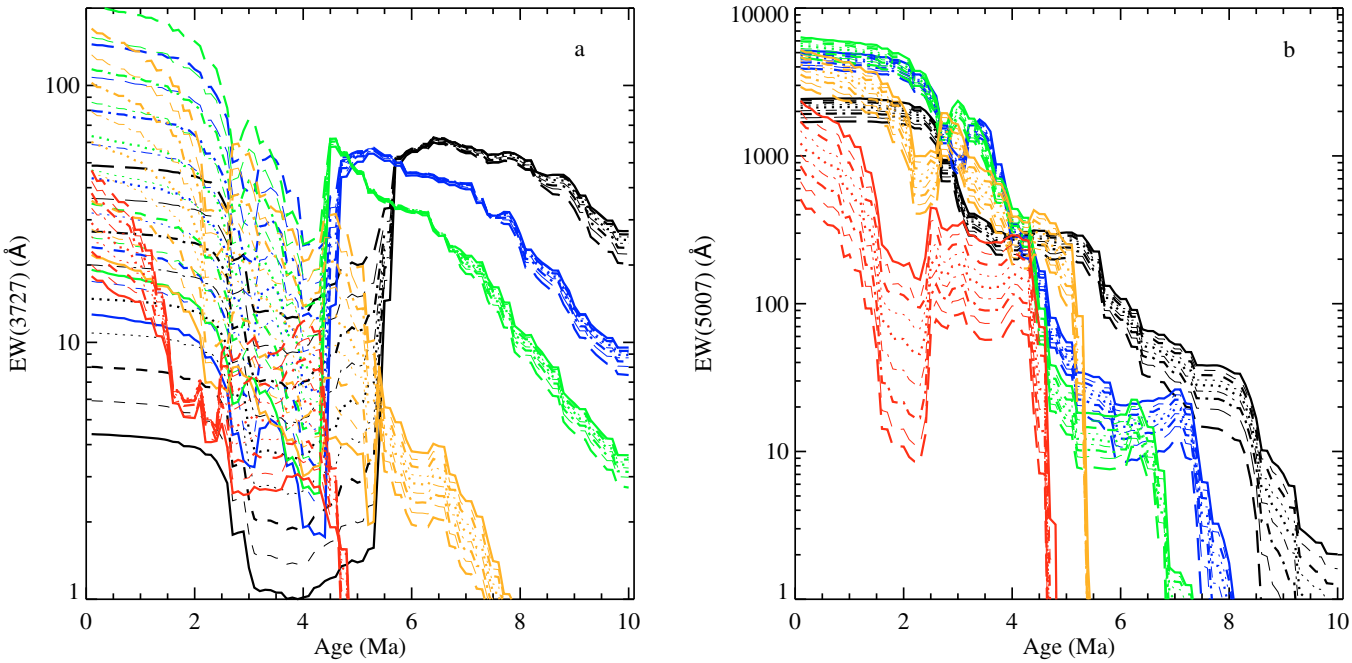

Fig. 6. Equivalent widths of **a)** [O II] λ 3727 Å; and **b)** [O III] λ 5007 Å for models with $M \geq 10^3$ $M_\odot$. Symbols as in Fig. 1.

(slopes different from 1). On the other hand, the *EW* is almost independent on the cluster mass for old ages.

[O II] λ 3727 Å and *EW*(3727) are used as star formation rate (SFR) indicators (Gallagher et al. 1989; Kennicutt 1992; Rosa-González et al. 2002, among others). The method is based on linear relations between [O II] λ 3727 Å and Hα or Hβ. Many authors have studied the dependence of these relations on the luminosity (Jansen et al. 2001; Aragón-Salamanca et al. 2003), the reddening (Rosa-González et al. 2002; Aragón-Salamanca et al. 2003) and abundances (Jansen et al. 2001; Kewley et al. 2004;

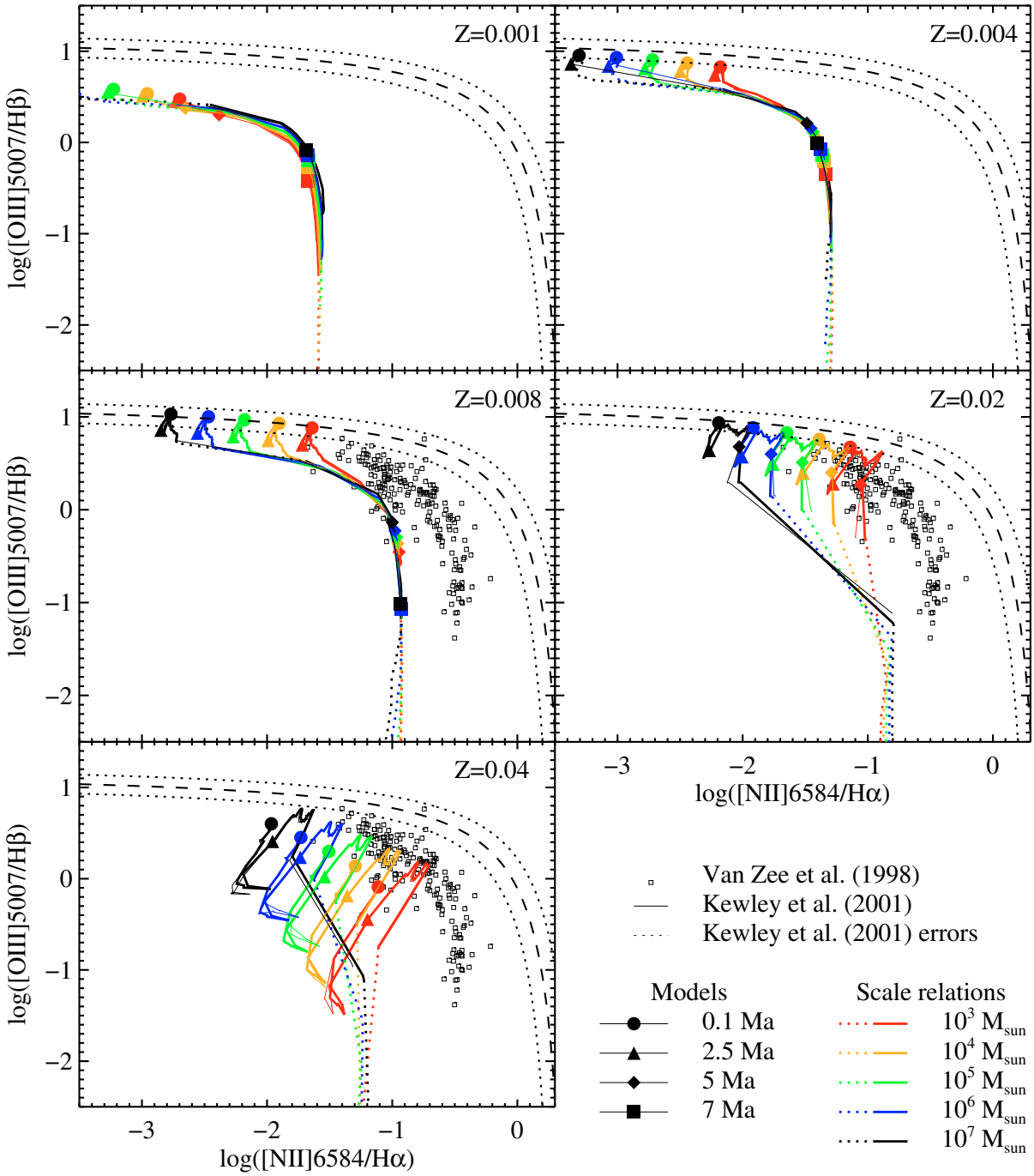

Fig. 7. [O III] 5007/Hβ vs. [N II] 6584/Hα diagnostic diagrams for each metallicity. Grey scale lines represent results from models and scale-relations for different cluster mass. Narrow lines with symbols represent the age evolution of models that fulfill the $EW > 1$ Å criteria; different symbols correspond to different ages. Dotted/solid lines are the results of applying the scale relations to the individual cluster masses, being the dotted part the region where the EW (as computed by Eq. (6)) of any of the lines involved is lower than 1 Å. For reference we also show van Zee et al. (1998) observations (open black squares), and the Kewley et al. (2001) curve (long dashed) with its error limits (short dashed curves).

Mouhcine et al. 2005; Moustakas et al. 2006). From the value of the slopes for [O II] λ 3727 Å and Hα (being the last similar to the ones shown in Fig. 4), we obtained that the [O II] 3727/Hα ratio roughly depends on $M^{-0.3}$ in the 0.1–4.5 Ma range, having a dependence flatter than $M^{0.05}$ for larger ages. Therefore at very early ages the SFR estimation has a non negligible dependence on the mass of the ionizing cluster of the observed H II regions. However, it is a good SFR indicator for older ages. Our study suggests that a recalibration of [O II] λ 3727Å using only old (age > 4.5 Ma) clusters would improve its use as an SFR indicator and that the method should be applied to galaxies dominated by H II regions older than 4.5 Ma.

It is noteworthy that the slope of [O III] λ 5007 Å is nearly 1. Considering all the metallicities except $Z = 0.04$ and ages lower than 7 Ma, we can adopt a value of 1.05 as a representative slope for this emission line. In such case we obtain $EW([\mathrm{O\,III}]\ 5007) \propto M^{0.05}$. Therefore EW([O III] 5007) seems to be a suitable age indicator as Stasińska & Leitherer (1996) had

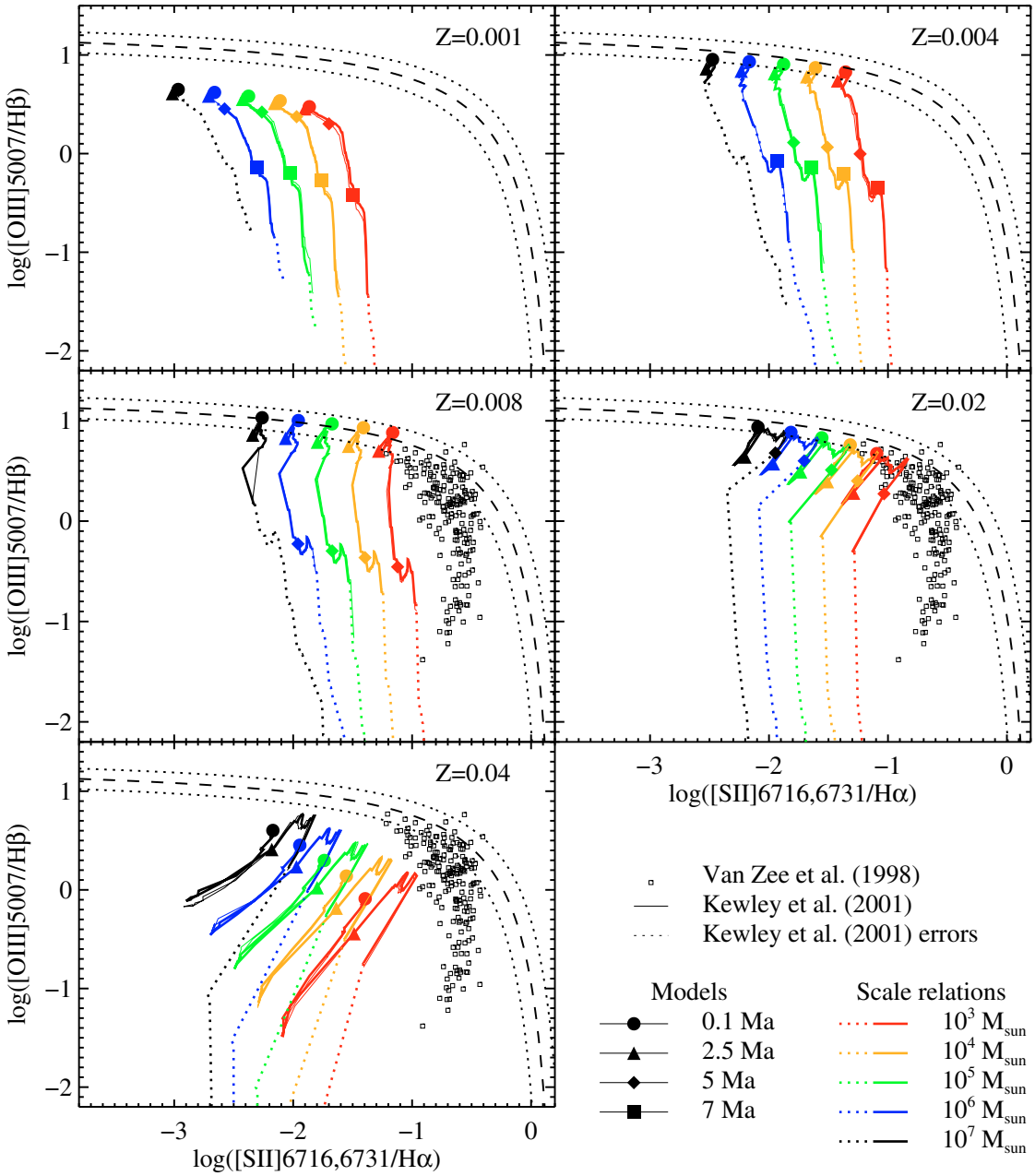

Fig. 8. O III 5007/Hβ vs. S II 6716,6731/Hα diagnostic diagrams for each metallicity. Symbols as in Fig. 7.

proposed. Nevertheless the dependence with the cluster mass is large enough to produce a non-negligible uncertainty in the age. This can be checked in Fig. 6b where the equivalent width of [O III] λ 5007 Å is shown. Comparing it with Fig. 1, it can be seen that the sequences for equal metallicity span a larger EW-range than for EW(Hβ). Moreover there are more situations of age degeneracy if [O III] λ 5007 Å is used. Therefore caution is needed when using this line for age estimations. In Fig. 6b it can also be seen that the age range for the application of EW([O III] 5007) as an age indicator is smaller than for EW(Hβ), because EW([O III] 5007), and therefore the detection of the line, decreases faster than EW(Hβ).

The slopes of [S II] λ 6716 Å are smaller than 1 except for $Z = 0.04$ at older ages. This means that the EW and ratios of [S II] λ 6716 Å with Hα and Hβ will decrease with increasing cluster mass.

The reliability of these scale-relations can be checked comparing the results obtained with them with the results obtained directly from the models. The comparisons have been made with some diagnostic diagrams and computing some relevant parameters. At the same time, clues of the influence of the cluster mass on such diagrams and parameters have been obtained.

3.2.1. Diagnostic diagrams

We have used two diagnostic diagrams to compare the scale-relations with the models. Let us remind that scale-relations built with models in the whole mass range (1–10^7 $M_\odot$) do not agree well with the results obtained directly from the models, especially in the high-mass range where the luminosity is overestimated. The inclusion of low mass clusters, which is just an academic case, produces a concave curvature in the $\log M - \log L$

plane, so the inclusion of low mass clusters produces a steeper slope (and a lower normalized luminosity). As we explain in Sect. 3.1.3 we primarily seek a good agreement in the high-mass range. For this reason our final scale-relations have been computed only with models with $M \geq 10^3\ M_\odot$. This clearly improves the results of scale-relations in the high-mass range; furthermore, we have also checked that for low masses the results are acceptable (though overestimated). In the following, we focus only on the simulations with clusters larger than $10^3\ M_\odot$.

In Fig. 7 the [O III] 5007/Hβ vs. [N II] 6584/Hα diagram proposed by Baldwin et al. (1981) is shown. Narrow lines with symbols represent the age evolution of models that fulfill the $EW > 1$ Å criterion. Different symbols correspond to different ages. Note that the models do not fulfill the EW for all ages (and they have not been plotted in such cases). Dotted/solid lines are the results of applying of the estimations of the line intensities with the scale relations obtained previously to the individual cluster masses, the dotted part being the ages where the EW of any of the lines involved in the diagram is lower than 1 Å. The theoretical upper limit for starbursts from Kewley et al. (2001) (black dashed line) and its estimated errors (black dotted line) are also shown for reference.

In general, there is a good agreement between the models and the results obtained using the scale relations, and there are only noticeable discrepancies for the $Z = 0.04$ case. It is also interesting to find in the $Z = 0.001$ case that only the less massive clusters produce EW([N II]) larger than 1. It is consistent with the results of Fig. 5, which show that, given the slope lower than 1 of the L([N II]) scale relation, the EW([N II]) decreases as the cluster mass increases for young ages. Our models and scale relations show that for fixed metallicity and $T_{\rm eff}$, i.e. constant age, there is a sequence in decreasing $Q(\mathrm{H}^0)$, or equivalently in decreasing mass. In general, models and scale relations have trends similar to, or at least compatible with, the observations.

Some of our scale-relations (and models) are slightly above the Kewley et al. (2001) curve. Such models correspond to clusters of $10^7\ M_\odot$ and metallicities in the 0.004–0.02 range. Kewley et al. (2001) estimated an error of ±0.1 dex due to potential errors in the modelling. Taking into account such errors, all our scale-relation estimations agree with the Kewley et al. (2001) limits.

In Fig. 8 the [O III] 5007/Hβ vs. [S II] 6716+6731/Hα diagnostic diagram is shown. The results estimated from the power-law scale-relations follow the trends of the models, and also reproduce some of the features (peaks, turn-off and EW) that the sequences of models present. The diagram shows clearly the effects of the cluster mass in the [S II] 6716+6731, which produce a serie of parallel sequences. Again, there is a good agreement between models and scale relations, with the larger discrepancies at $Z = 0.04$. Scale relations show that it is more difficult to detect the [S II] lines in more massive clusters. Since the slope in the $\log M - \log L$ relation is almost constant for all ages and lower than one, both the [S II] 6716+6731/Hα and the EW of the line decreases with increasing cluster mass. In this diagram, observations and models/scale relations have a poorer agreement than in the [O III] 5007/Hβ vs. [N II] 6584/Hα diagram. However, notice that [S II] $\lambda\lambda$ 6716, 6731 Å, as [O I] λ 6300 Å, are likely to be affected by shocks and since Cloudy does not include shocks, the results for those lines are not complete.

From these comparisions we conclude that, although not perfect, the scale-relations are suitable tools for cluster masses larger than $10^3\ M_\odot$.

3.2.2. The η parameter, R_{23} and S_{23}

The η parameter was defined by Vílchez & Pagel (1988) as:

$$\eta = \frac{\mathrm{O}^+/\mathrm{O}^{++}}{\mathrm{S}^+/\mathrm{S}^{++}}\ , \tag{7}$$

and it is related with the observational ratio:

$$\eta' = \frac{[\mathrm{O\,II}]\ 3727 + 3729/[\mathrm{O\,III}]\ 4959 + 5007}{[\mathrm{S\,II}]\ 6717 + 6731/[\mathrm{S\,III}]\ 9069 + 9532}\ . \tag{8}$$

The slopes of the scale-relations computed for each of the lines involved in the ratio can be used to estimate the η' dependence on mass. As can be seen in Fig. 5, for each line the computed slopes have similar values and trends for all metallicities except for $Z = 0.04$. Thus, as a rough approximation, we can define for each line a representative slope and obtain the following proportionalities valid for all the metallicities considered except for $Z = 0.04$:

$$I([\mathrm{O\,II}]3727) \propto \begin{cases} M^{0.75} & \text{if} \quad \text{age} < 4.5\ \text{Ma}, \\ M^{1.03} & \text{if} \quad \text{age} > 4.5\ \text{Ma}; \end{cases} \tag{9}$$

$$I([\mathrm{O\,III}]5007) \propto M^{1.05}; \tag{10}$$

$$I([\mathrm{S\,II}]6716) \propto M^{0.73}; \tag{11}$$

$$I([\mathrm{S\,III}]9069) \propto \begin{cases} M^{0.77} & \text{if} \quad \text{age} < 4.5\ \text{Ma}, \\ M^{1.03} & \text{if} \quad \text{age} > 4.5\ \text{Ma}. \end{cases} \tag{12}$$

[O III] λ 4959 Å, [S II] λ 6731 Å and [S III] λ 9532 Å present dependences with the cluster mass similar to their associated lines from above. Using these proportionalities we obtain for η':

$$\eta' \propto \begin{cases} M^{-0.26} & \text{if} \quad \text{age} < 4.5\ \text{Ma}. \\ M^{0.28} & \text{if} \quad \text{age} > 4.5\ \text{Ma}. \end{cases} \tag{13}$$

These trends can be seen in Fig. 9 where η' versus $\log(Z)$ is represented for each cluster mass. The grey scale colors, unlike in previous figures, indicate the age. Results obtained directly from models are shown with circles connected by narrow lines. We have only plotted the models that fulfil the EW criteria. Results computed with scale-relations are represented with dotted/solid lines with a larger line weight. Dotted parts of the lines connect metallicity points where either point does not fulfill the EW criteria as obtained by the scale laws. The agrement within the models and scale relations is remarkable. At ages lower than 4.5 Ma, scale-relations produce η' values that decrease with increasing mass, while at larger ages η' increases with mass. This behaviour is due to the variation of the scale relation of the [S III] and [O II] lines.

The R_{23} parameter was proposed as an abundance calibrator by Pagel et al. (1979), and is defined as:

$$R_{23} = \frac{[\mathrm{O\,II}]\ 3727 + [\mathrm{O\,III}]\ 4959 + 5007}{\mathrm{H}\beta}\ . \tag{14}$$

Following the same method as for η', we estimate the dependence of R_{23} with the cluster mass. Taking into account that H$\beta \propto M$ and using Eqs. (9) and (10), we obtain:

$$R_{23} \propto \begin{cases} A_{R23} M^{-0.25} + B_{R23} M^{0.05} & \text{if} \quad \text{age} < 4.5\ \text{Ma}. \\ A_{R23} M^{0.03} + B_{R23} M^{0.05} & \text{if} \quad \text{age} > 4.5\ \text{Ma}. \end{cases} \tag{15}$$

where the A_{R23} and B_{R23} factors are obtained from the intensity of the lines used in R_{23} normalized to the total mass, therefore they depend on age and metallicity.

Recalling that the continuum has a slope equal to 1 (see Sect. 3.1.3) the same result is obtained if the EW of the lines are used as Kobulnicky & Phillips (2003) proposed.

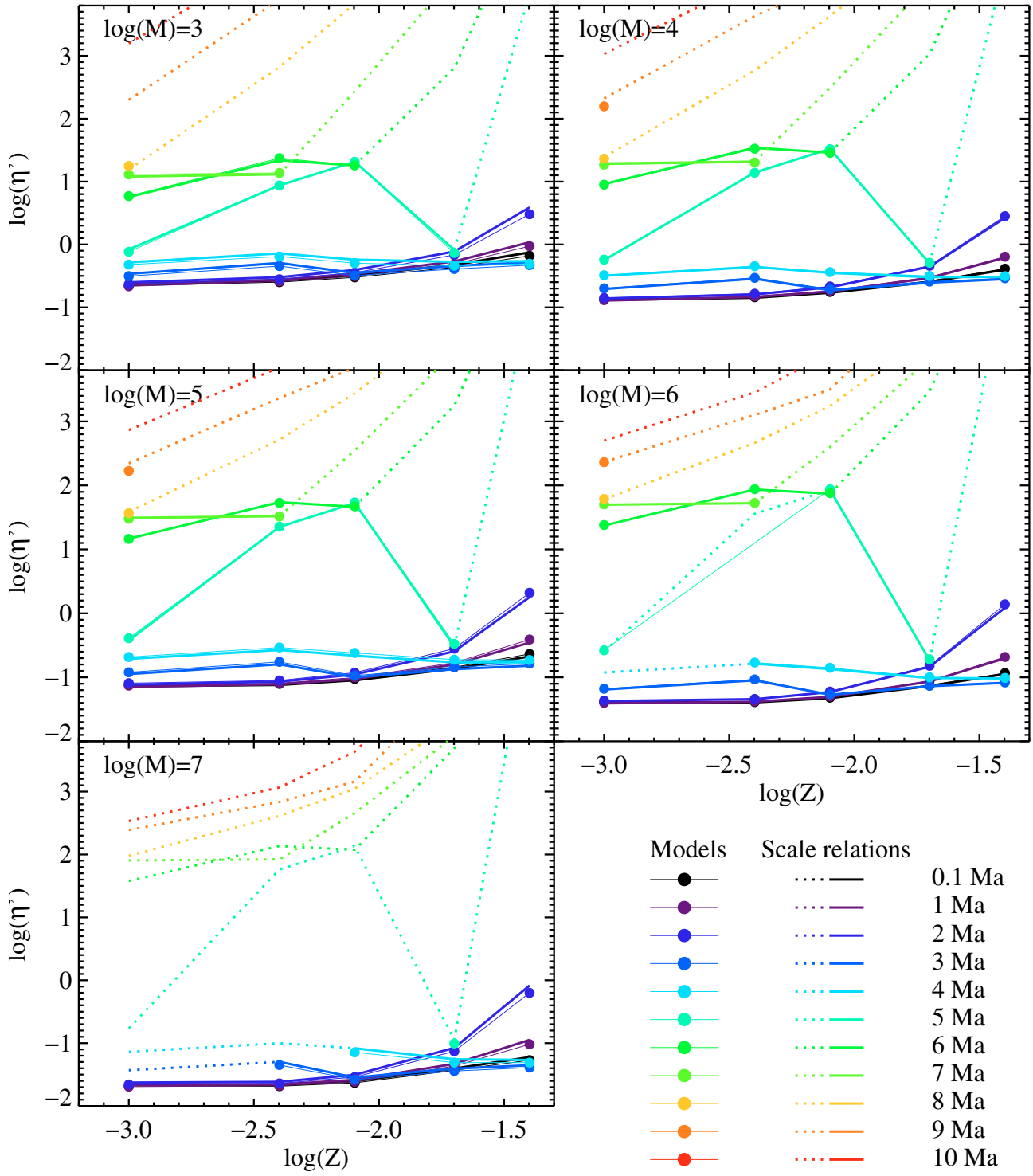

Fig. 9. η' parameter computed with scale-relations (dotted/solid broad lines) and models (narrow lines) for each cluster mass. Grey scale colors represent ages.

In Fig. 10 the values obtained for R_{23} are shown. The dependence in mass estimated above, in spite of being small, can be appreciated when comparing carefully the plots for different masses. The agreement between scale-relations and models is better than for the η' parameter.

The S_{23} parameter was defined by Vílchez & Esteban (1996) in a way similar to R_{23}:

$$S_{23} = \frac{[\mathrm{S\,II}]6717 + 6731 + [\mathrm{S\,III}]9069 + 9532}{\mathrm{H}\beta}\,. \tag{16}$$

For this parameter we obtain a mass dependence of the form:

$$S_{23} \propto \begin{cases} A_{S23} M^{-0.27} + B_{S23} M^{-0.23} & \text{if} \quad \text{age} < 4.5\ \text{Ma}. \\ A_{S23} M^{-0.27} + B_{S23} M^{0.03} & \text{if} \quad \text{age} > 4.5\ \text{Ma}. \end{cases} \tag{17}$$

where the A_{S23} and B_{S23} factors depend on age and metallicity.

As R_{23}, S_{23} also shows a dispersion of the results of the models due to different cluster masses (see Fig. 11). A relevant fact is the variation of S_{23} with the age through the mass range. As the mass increase the sequences for older ages rise and the lower

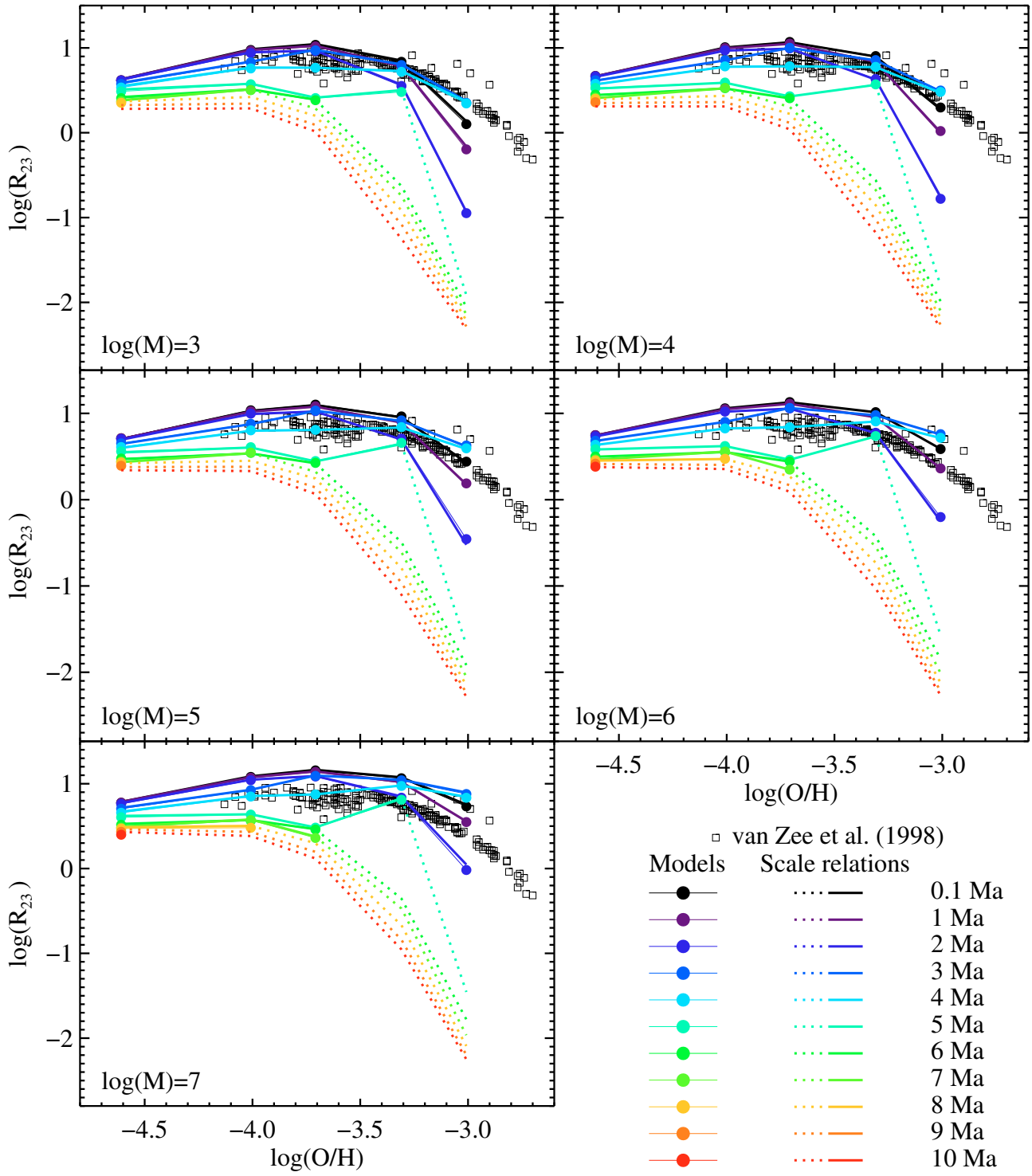

Fig. 10. R_{23} for each cluster mass. Black squares: van Zee et al. (1998) observations. Rest of symbols as in Fig. 9.

ages ones go down. This behaviour can be explained with the different dependences of S_{23} with the mass for ages below and over 4.5 Ma.

4. Summary of results and discussion

Using models of H II region ionized by clusters of different masses, we have studied the variation of the H II region emission with the ionizing cluster mass. For this task, scale-relations in form of power-laws between the intensities of some of the most relevant emission lines and the ionizing cluster mass have been obtained. The reliability of these power-law scale-relations has been checked by means of diagnostic diagrams. We check that the general agreement between power-law scale-relations and models is better if we compute the power-laws using only the models with $M \geq 10^3\ M_\odot$, with the intensities of collisional lines being overestimated by the power law relations in the case of clusters with masses lower than $10^3\ M_\odot$. However, the ionizing flux of such low mass clusters cannot be described by the average ionizing flux obtained by synthesis models (cf. Paper I).

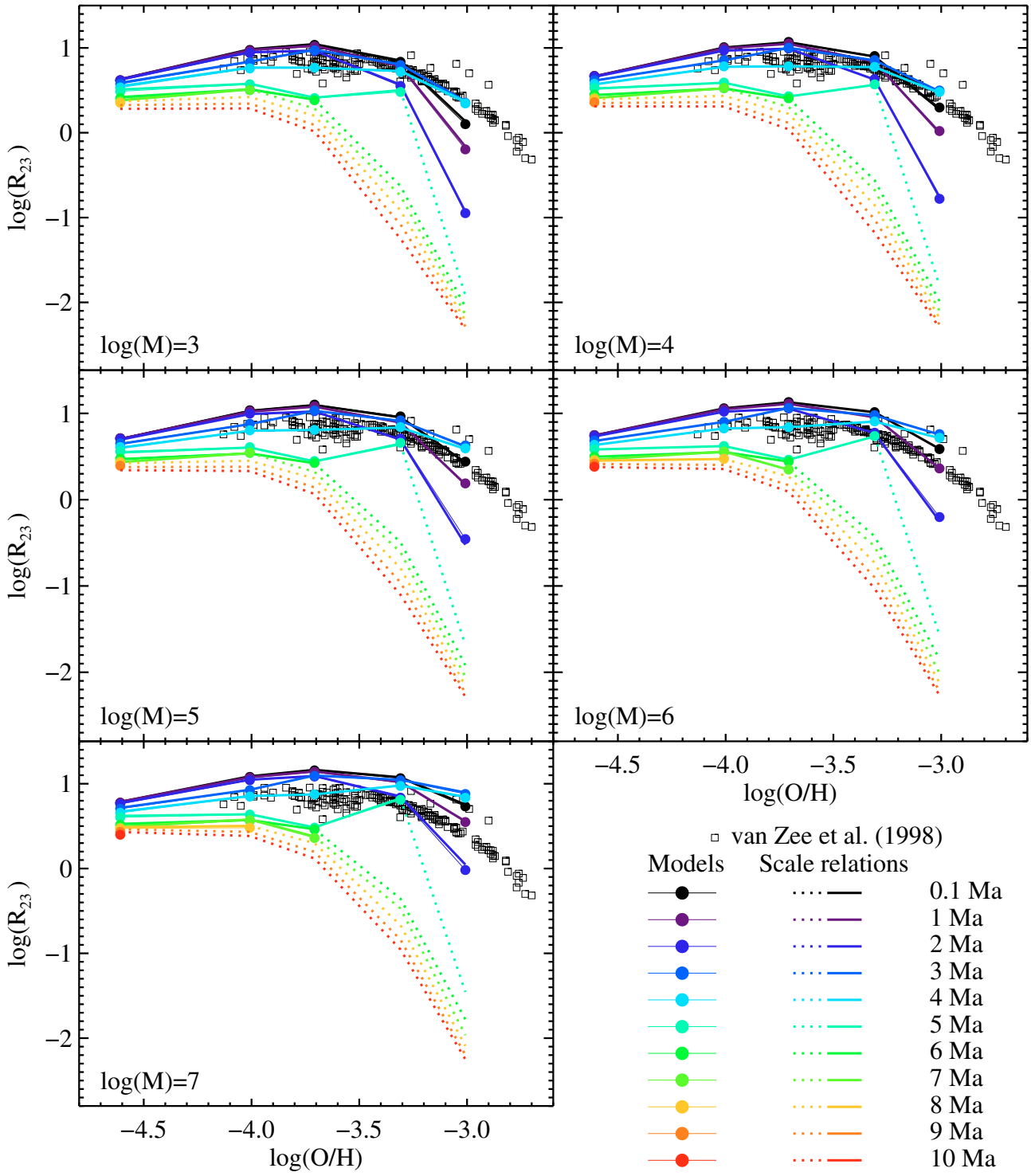

Fig. 11. S_{23} for each cluster mass. Symbols as in Fig. 9.

We want to stress that, due to the assumptions in the modelling and the simple linear approximation, these scale-relations are just a partial first approach from which we can obtain an overall view of the dependence of line intensities with the cluster mass, but these scale relations must not be used as an *exact* representation of the variation of the intensities of the emission lines with the cluster mass. In this sense, our scale-relations, although incomplete, are very useful tools that describe *mean* luminosity functions. Therefore they could be used when considering the mass dependence of the properties of massive H II regions samples, but should not be applied to individual objects. An example of the limitations of our scale-relations is that they cannot predict the variation of the Hα/Hβ variation of the models with respect to the normally assumed value, variation that induce a spurious extinction effect.

In spite of these limitations, simply estimating the trend of the luminosity distribution function allows to make interesting predictions. The exponents of the power-law scale-relations indicate us the mass dependence of the line luminosity. With this dependence it is possible to estimate the influence of the cluster

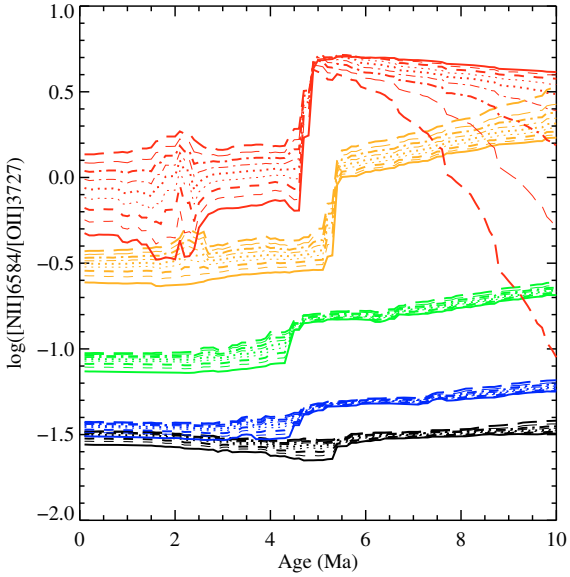

Fig. 12. The [N II] 6584/[O II] 3727 ratio versus age for clusters with $M \geq 10^3$. Symbols as in Fig. 1.

mass on *EW*s and on some relevant line intensities ratios. If a quantity has no dependence on cluster mass it can be calibrated with observations with no need of age and cluster mass estimations, otherwise a correction in mass should be applied. We check that $EW(\mathrm{H}\beta)$ is almost insensitive to mass, while EW([O III] 5007) has a small dependence. This implies that EW([O III] 5007) is not as good as an age indicator as $EW(\mathrm{H}\beta)$, and that we have to take into account the cluster mass when estimating ages with EW([O III] 5007). We also explore the variation of EW([O II] 3727) with mass cluster and we obtain an important mass dependence for ages lower than ∼4.5 Ma, depending on metallicity, and almost no mass dependence at older ages. The different mass dependences of [O II] λ 3727 Å, [O III] λ 5007 Å, and therefore of their *EW*s, offer a possible explanation for the different dispersions in their respective $\log(EW/EW(\mathrm{H}\beta))$ vs. $\log(\mathrm{I}/\mathrm{I}(\mathrm{H}\beta))$ plots (Kobulnicky & Phillips 2003). The mass dependence of the [O II] 3727/Hα ratio, similar to EW([O II] 3727), implies that the [O II] λ 3727 Å intensity is not a good SFR indicator if clusters with ages lower than 4.5 Ma are present. This suggests that the [O II] λ 3727 Å intensity should be recalibrated and that its use should be limited to galaxies dominated by H II regions older than 4.5 Ma.

The power-law scale-relations also allow us to identify emission line ratios with small mass dependence. This is the case of [O II] 3727/[N II] 6584 ratio, proposed as an abundance indicator by van Zee et al. (1998) and Dopita et al. (2000). The values and behaviour of the slopes for these two lines are similar, with greater differences at the highest metallicities. Therefore their ratio will have a small mass dependence at any age. This can be seen in Fig. 12, where the [N II] 6584/[O II] 3727 ratio is plotted versus the age. The thin sequences obtained for low metallicities account for the small mass dependence. This clearly helps to separate the sequences for differents metallicities, allowing a better abundance estimation. The drop of [N II] 6584/[O II] 3727 for $Z = 0.040$ (long-dashed red line) at ages older than 6 Ma is due to a higher contribution of recombination emission to the [O II] λ 3727 Å luminosity.

The scale-relations have been used together with the definition of some parameters (η', R_{23} and S_{23}) in order to estimate their dependence with the cluster mass. For η' and S_{23} the models show variations of these ratios with the cluster mass that, in spite of the strong assumptions in the modelling, stress the need of taking into account the mass of the ionizing clusters when estimating physical properties from these ratios. For $M \geq 10^3\ M_\odot$, η' and S_{23} have opposite mass dependences at ages earlier and older than 4.5 Ma. On the other hand, R_{23} shows almost no dependence on mass. In this sense, R_{23} seems a quite robust indicator. Moreover, it also means that R_{23} could be calibrated without having to worry about the mass of the ionizing clusters, and therefore objects of different masses can be used together in its calibration.

Additionally, the scale relations allow us to estimate when an emission line can be detected taking into account the continuum level. It turns out that it is easier to detect emission lines in low mass clusters when the scale relations have slopes lower than one.

It can be argued that the variation with the cluster mass can also be described by variations of other parameters, but the use of the mass as a parameter allow to use directly the synthesis models and an easier approach to other properties parameterized with the mass (as the star formation history) and to the the IMF sampling problem. Moreover, implementing the mass dependence in the calibration of an estimation method would improve the estimations. Since including the cluster mass in H II region models is a non-trivial task, and it is not a sufficiently studied issue, the theoretical calibrations of estimation methods with mass dependent indicators should be used with extra caution. Therefore empirical or semi-empirical calibrations would work better than theoretical ones since the former consider in a natural way the variation in the cluster mass, although it is necessary to estimate the mass by alternative methods (e.g. star counts or dynamic effects).

As we have said, our models and scale-relations are less realistic for the lowest masses ($M \leq 10^3\ M_\odot$). To improve the reliability in general, and in the low mass range in particular, an estimation of the influence of sampling effects of the stellar IMF is needed (Cerviño & Mas-Hesse 1994; Cerviño et al. 2000, 2002b, 2003; Cerviño & Luridiana 2006). This would allow to describe properly the possible distribution of the cluster ionizing continua. Such distribution for low mass clusters has a large dispersion and bimodality in $T_{\rm eff}$ (Villaverde et al. 2009). That imply that there could be low mass clusters with an ionizing flux equal or greater than a larger mass cluster. The effects of the dispersion of $T_{\rm eff}$ for low mass clusters on the H II region spectra are treated on Villaverde et al. (2009) to which the reader is referred.

We can obtain the same back-of-the-envelope estimation of the influence of low mass clusters on the emission line spectra of a non-active galaxy, and obtain a first order check of the statement by Dopita et al. (2006b) on the lack of influence of low mass clusters (and hence, sampling effects) on the total line flux of collisional lines. Dopita et al. (2006a) assume a lognormal ICMF

$$P(M) = \frac{1}{M\sigma\sqrt{2\pi}} \mathrm{e}^{\left(-\frac{(\ln M-\mu)^2}{2\sigma^2}\right)}, \tag{18}$$

with $\sigma = 1.7$ and $\mu = \ln 100\ M_\odot$. Such a distribution has a mean about 424 $M_\odot$, a median equal to 100 $M_\odot$ and a mode (maximum value) about 5 $M_\odot$. However, in Dopita et al. (2006a) they argued than they only make use of this distribution for cluster masses larger than $10^3\ M_\odot$ and that massive cluster wash out the stochastic effects.

We test their statement by computing the fraction of the total luminosity of the emission line that is produced by clusters

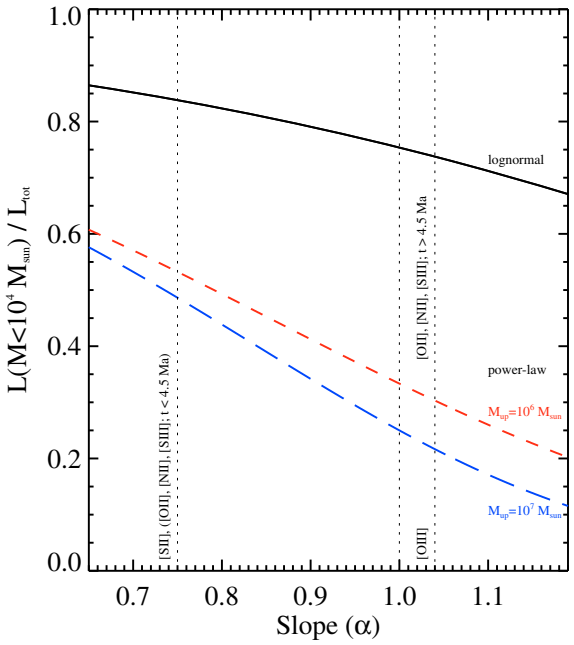

Fig. 13. Contribution of clusters less massive than 10^4 $M_\odot$ to the total luminosity as a function of the slope of the mass luminosity relation for different ICMF recipes.

with mass less than $M_x = 10^4$ $M_\odot$. The use of 10^4 $M_\odot$ instead of 10^3 $M_\odot$ is because for 10^3 $M_\odot$ clusters, synthesis models includes stars more luminous than the cluster itself (the Lowest Luminosity Limit, see Cerviño et al. 2003; Cerviño & Luridiana 2004, for details), so at such masses there is not only a sampling effect problem, but a physical one in the modeling. Clusters in the 10^3–10^4 $M_\odot$ are still affected by sampling effects with luminosity distributions that are not Gaussian (cf. Cerviño & Luridiana 2006), so we take 10^4 $M_\odot$ as a conservative lower limit for clusters affected by sampling. The integration of a lognormal ICMF with a power-law mass dependent luminosity is:

$$\int AM^\alpha P(M)\,\mathrm{d}M = -\frac{A}{2}e^{\alpha\mu+\frac{\alpha^2\sigma^2}{2}}\,\mathrm{Erf}\left[\frac{\mu+\alpha\sigma^2-\ln M}{\sqrt{2}\sigma}\right] \qquad (19)$$

with Erf(x) the Gaussian error function. Hence, the contribution of clusters less massive than M_x as a function of the slope of the mass-luminosity relation is:

$$\frac{L(M<M_x)}{L_{\rm tot}} = \frac{\mathrm{Erf}\left[\frac{\mu+\alpha\sigma^2-\ln M_{\rm low}}{\sqrt{2}\sigma}\right]-\mathrm{Erf}\left[\frac{\mu+\alpha\sigma^2-\ln M_x}{\sqrt{2}\sigma}\right]}{\mathrm{Erf}\left[\frac{\mu+\alpha\sigma^2-\ln M_{\rm low}}{\sqrt{2}\sigma}\right]-\mathrm{Erf}\left[\frac{\mu+\alpha\sigma^2-\ln M_{\rm up}}{\sqrt{2}\sigma}\right]}\,. \qquad (20)$$

We have also computed the same quantity for the case of a power-law ICMF,

$$P(M) = C_{\rm cl}M^{-\alpha_{\rm cl}}, \qquad (21)$$

which produces the following contribution of clusters less massive than M_x as a function of the slope of the mass-luminosity relation:

$$\frac{L(M<M_x)}{L_{\rm tot}} = \frac{M_{\rm low}^{1+\alpha-\alpha_{\rm cl}}-M_x^{1+\alpha-\alpha_{\rm cl}}}{M_{\rm low}^{1+\alpha-\alpha_{\rm cl}}-M_{\rm up}^{1+\alpha-\alpha_{\rm cl}}}\,. \qquad (22)$$

Figure 13 shows the variation of the contribution of clusters less massive than M_x to the total luminosity as a function of the slope α of the mass-luminosity relation. The approximative values of α for different lines has been drawn as vertical lines. We have also assumed a $M_{\rm low} = 10^3$ $M_\odot$ and a $M_{\rm up} = 10^6, 10^7$ $M_\odot$ as limits of the ICMF. In the case of a lognormal ICMF as proposed by Dopita et al. (2006b), the figure shows that clusters in the 10^3–10^4 $M_\odot$ range are responsible for more than 70% of the luminosity of the [O III] emission lines for all ages (and [O II], [S III] and [N II] at ages larger than 4.5 Ma). This contribution is larger than 80% for [S II] in all the age range (and [O II], [S III] and [N II] at ages lower than 4.5 Ma). This result is independent of the choice of the $M_{\rm up}$: the high mass tail of the lognormal distribution is steeper than the one of power law distributions, so high mass clusters have a low impact on the total flux, in opposition to Dopita et al. (2006a) assumption. In this situation, the statement by Dopita et al. (2006a) is clearly wrong.

We have also show the case of a ICMF described by a power law with exponent $\alpha_{\rm cl} = 2$. In this situation, the contribution of massive clusters to the total luminosity is more important with a significant dependence of the choice of $M_{\rm up}$ in the ICMF. However, the contribution of low mass clusters to some of the emission lines ([O II], [S III] and [N II] at ages smaller than 4.5 Ma) is around 50%, and only around 20% for [O III] for all ages and [O II], [S III] and [N II] at ages larger than 4.5 Ma.

Although we have not taken into account either the star formation history or clusters less massive than 10^3 $M_\odot$ in this calculations, it is enough to prove that the statement about the washing out of the stochastic effects of low mass cluster by Dopita et al. (2006b) needs to be revised in detail. This subject will be addressed in another work.

Finally, we have compared our scale-relations with the Stasińska et al. (2001) models. Those models considered several different values for density and filling factors, moreover the inner radius varies from model to model. For a consistence check we have only considered instantaneous burst models with IMF upper stellar mass similar to ours. In Figs. 14–16 the intensities of some of the most relevant emission lines versus the Hβ intensity are shown. Since the intensity of Hβ is proportional to the mass, the tendencies shown in these plots can be directly compared to the slopes of our scale-relations. Only the models that have an age, mass and metallicity for which our scale-relations predict $EW \geq 1$ are plotted. Models with ages lower and greater than 4.5 Ma are plotted separately, because around that age many lines show a sudden change in their scale-relations slopes. Lines with slope equal to 1 and representative slopes from the scale-relations are shown as a reference for each emission line and age interval. The zero-point of these reference lines has been adjusted for a better comparison with models. For [O II] λ 3727 Å and ages lower than 4.5 Ma the models follow a tendency with slope smaller than 1, while for older ages the slope is near 1. These tendencies coincide with the ones obtained with our scale-relations (see Fig. 5). The same occurs for [O III] λ 5007 Å and [N II] λ 6584 Å (Figs. 15 and 16). Moreover, the scatter in the plots, which is due to the different ages, metallicities and physical parameters of the models, corresponds to the spread of values of the α coefficient of the scale-relations. These similar tendencies indicate that our scale-relations are robust against changes of density, inner radius and filling factor.

5. Conclusions

In this work we have studied the variation of the H II regions spectrum with the ionizing cluster mass. For this task we have done photoionization models for several metallicities and ages

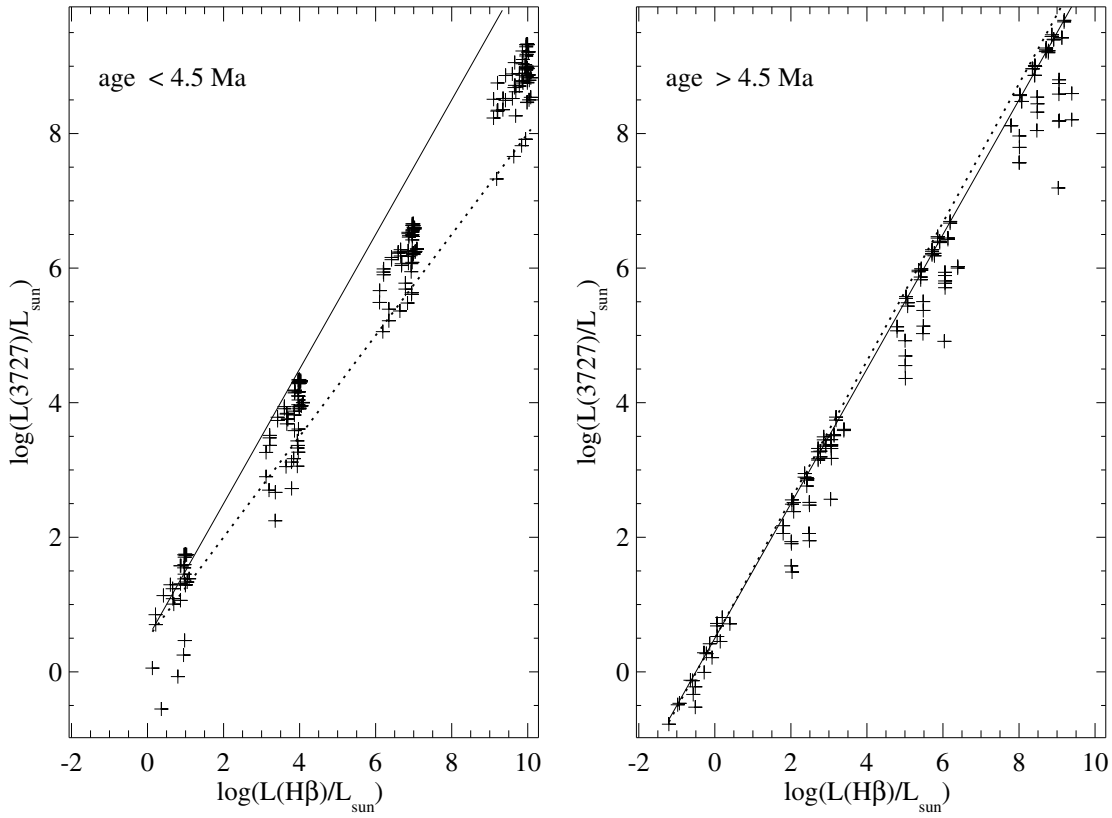

Fig. 14. [O II] λ 3727 Å/luminosity with respect to the Hβ luminosity for Stasińska et al. (2001) models with ages lower (*left*) and higher (*right*) than 4.5 Ma. A solid line with slope equal to 1 and dotted lines with representative slopes are shown as references.

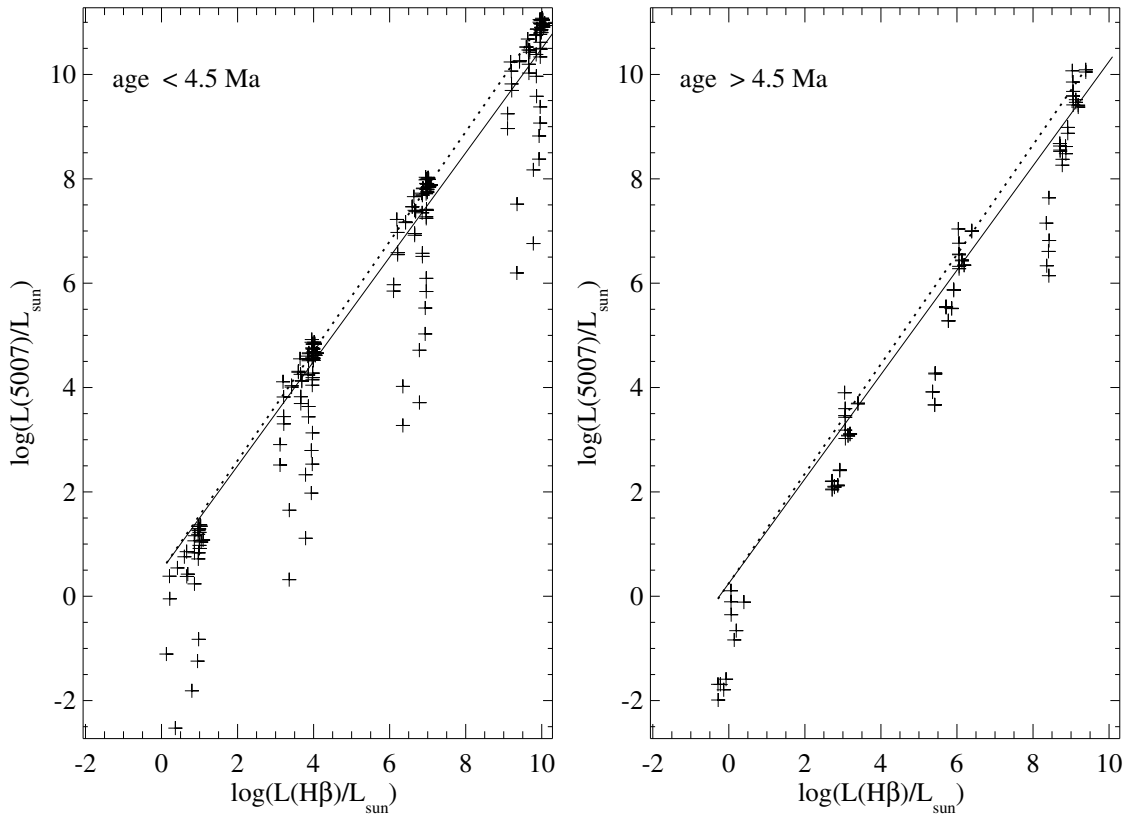

Fig. 15. [O III] λ 5007 Å/luminosity with respect to the Hβ luminosity for Stasińska et al. (2001) models with ages lower (*left*) and higher (*right*) than 4.5 Ma. A solid line with slope equal to 1 and dotted lines with representative slopes are shown as references.

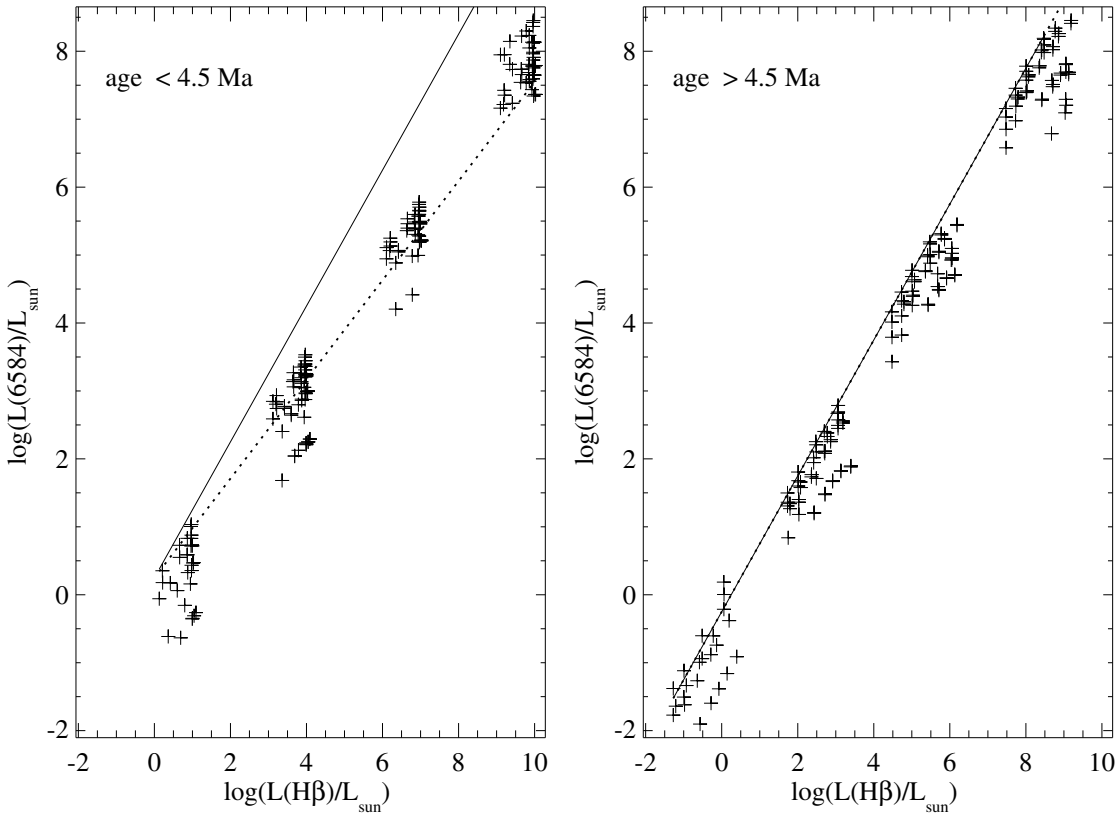

Fig. 16. [N II] λ 6584 Å/luminosity with respect to the Hβ luminosity for Stasińska et al. (2001) models with ages lower (*left*) and higher (*right*) than 4.5 Ma. A solid line with slope equal to 1 and dotted lines with representative slopes are shown as references.

in a cluster mass range from 10^3 to 10^7 $M_\odot$. From these models we obtain power-law scale-relations between the emission line intensities and the ionizing cluster mass.

These power-law scale-relations are very useful tools since they allow to estimate in a simple way mass dependences of EW and line intensities ratios. Using such scale-relations we have checked that EW(Hβ) is practically independent of mass, a result which supports its use as an age indicator. On the other hand, EW([O III] 5007) has a mass dependence that, in spite of being small, implies that some caution is needed when using it as an age indicator. The mass dependence obtained for [O II] λ 3727 Å implies that it is a good SFR indicator if it is calibrated with H II regions older than 4.5 Ma, and used on objects dominated by such H II regions. As the mass dependence of [O II] λ 3727 Å is similar to the mass dependence of [N II] λ 6584 Å, the intensity ratio of these lines has a small mass dependence. This supports the use of that ratio as an abundance indicator. We also check that the R_{23} parameter is almost independent of mass, while S_{23} and η' have a non-trivial mass dependence.

The estimation methods that use mass independent indicators can be calibrated with no consideration for the mass of the objects. If the indicator is mass dependent, however, the estimation method should be recalibrated taking into account the ionizing cluster mass. For those methods, semi-empirical calibrations are, at least for now, more appropriate.

An additional result obtained from our models is an intrinsic limit of about $\Delta E(B-V) = 0.1$ in the accuracy of the extinction estimations carried out under the hypothesis assumed in synthesis models (case B and $T_e = 10^4$ K). This error is diminished if tailored models are used.

Finally, we have shown that the relevant collision lines have a non linear dependence with the cluster mass, and that, in general, not all the collisional lines have the same dependence (slopes in the $\log M - \log L$ differs from line to line). A direct implication of this result is that different collisional lines in the emission line spectrum of a non-active galaxy have different contributions from different HII regions and, hence, it depends on the HII population in the galaxy (and the underlying initial mass cluster distribution) and that low mass clusters ($<10^4$ $M_\odot$) can contribute more than 50% of the luminosity of the line. In this situation, any attempt to infer physical properties from the emission line spectrum of a non-active galaxy by comparison with single nebulae photoionization models and without taking into account the IMF sampling effects may be a risky business.

Acknowledgements. We thank the referee B. Groves for his patient and his comments, which had improve the paper. This work has been supported by the Spanish *Programa Nacional de Astronomía y Astrofísica* through FEDER funding of the project AYA2004-02703 and AYA2007-64712.

References

Allende Prieto, C., Lambert, D. L., & Asplund, M. 2001, ApJ, 556, L63
Allende Prieto, C., Lambert, D. L., & Asplund, M. 2002, ApJ, 573, L137
Anders, E., & Grevesse, N. 1989, Geochim. Cosmochim. Acta 53, 197
Aragón-Salamanca, A., Alonso-Herrero, A., Gallego, J., et al. 2003, ASP Conf. Ser., 297
Baldwin, J., Phillips, M. M., & Terlevich, R. 1981 PASP, 93, 5
Beckman, J. E., Rozas, M., Zurita, A., Watson, R. A., & Knapen, J. H. 2000 AJ, 119,2728
Carigi, L., & Hernández, X. 2008 MNRAS, 390, 582
Castellanos, M., Díaz, Á. I., & Tenorio-Tagle, G. 2002 ApJ, 565, 79
Cerviño, M., & Luridiana, V. 2004, A&A, 413, 145
Cerviño, M., & Luridiana, V. 2006, A&A, 451, 475
Cerviño, M., & Mas-Hesse, J. M. 1994, A&A, 284, 749
Cerviño, M., & Mollá, M. 2002, A&A, 394, 525
Cerviño, M., & Valls-Gabaud, D. 2003, MNRAS, 338, 481
Cerviño, M., Luridiana, V., & Castander, F. J. 2000, A&A, 360, L5

Cerviño, M., Mas-Hesse, J. M., & Kunth, D. 2002a, A&A, 392, 19
Cerviño, M., Valls-Gabaud, D., Luridiana, V., & Mas-Hesse, J. M. 2002b, A&A, 381, 51
Cerviño, M., Luridiana, V., Pérez, E., Vílchez, J. M., & Valls-Gabaud, D. 2003, A&A, 407, 177 (Paper I)
Charbonnel, C., Meynet, G., Maeder, A., Schaller, G., & Schaerer, D. 1993, A&AS, 101, 415
Charlot, S., & Longhetti, M. 2001, MNRAS, 323, 887
Copetti, M. V. F., Pastoriza, M. G., & Dottori, H. A. 1986, A&A, 156, 111
Dopita, M. A., Kewley, L. J., Heisler, C. A., & Sutherland, R. S. 2000 ApJ, 542, 224
Dopita, M. A., Fischera, J., Sutherland, R. S., et al. 2006a, ApJ, 647, 244
Dopita, M. A., Fischera, J., Sutherland, R. S., et al. 2006b ApJS, 167, 177
Ferland, G. J. 2003, ARA&A, 41, 157
Ferland, G. J. 2008, Hazy, A Brief Introduction to Cloudy, version 08, Univ. of Kentucky, Internal Report
Ferland, G. J., Korista, K. T., Verner, D. A., et al. 1998, PASP, 110, 761
Gallagher, J. S., Bushouse, H., & Hunter, D. A. 1989 AJ, 97, 700
García-Vargas, M. L., & Díaz, Á. I. 1994, A&AS, 91, 553
García-Vargas, M. L., Bressan, A., & Díaz, Á. I. 1995a, A&AS, 112, 13
García-Vargas, M. L., Bressan, A., & Díaz, Á. I. 1995b, A&AS, 112, 35
Grevesse, N. 1991, Evolution of Stars: the Photospheric Abundance Connection, IAU Symp., 145, 63
Grevesse, N., & Anders, E. 1989, AIP Conf. Proc. 183: Cosmic Abundances of Matter, 1
Grevesse, N., & Noels, A. 1993, in Origin & Evolution of the Elements, ed. N. Prantzos, E. Vanfioni-Flam, & M. Case (Cambridge Univ. Press), 15
Grevesse, N., Lambert, D. L., Sauval, A. J., van Dishoek, E. F., Farmer, C. B., & Norton, R. H. 1991, A&A, 242, 488
Huchra, J. P. 1977, ApJ, 217, 928
Iglesias-Páramo, J., & Muñoz-Tuñón, C. 2002 MNRAS, 336,33
Jamet, L., & Morisset, C. 2008, A&A, 482, 209
Jansen, R. A., Franx, M., & Faricant, D. 2001 ApJ, 551, 825
Kennicutt, R. C. 1992, ApJ, 388, 310
Kewley, L. J., Dopita, M. A., Sutherland, R. S., Heisler, C. A., & Trevena, J. 2001, ApJ, 556, 121
Kewley, L. J., Geller, M. J., & Jansen, R. A. 2004 AJ, 127, 2002
Kobulnicky, H. A., & Phillips, A. C. 2003 ApJ, 599,1031
Kurucz, R. L. 1991, in Stellar Atmospheres, Beyond Clasical Limits, ed. Crivellari L., Hubeny I., Hummer D. G. (Dordrecht: Kluwer), 441 (http://kurucz.harvard.edu/grids/)
Lada, C. J., & Lada, E. A. 2003, ARA&A, 41, 57
Leitherer, C., & Heckman, T. M. 1995, ApJS, 96, 9
Luridiana, V. 2009 in Young massive star clusters, Granada 2007, ed. E. Pérez, R., de Grijs, R. M. González Delgado, & S. Goodwin, in press
Luridiana, V., & Peimbert, M. 2001, ApJ, 553, 633
Luridiana, V., Peimbert, M., & Leitherer, C. 1999, ApJ, 527, 110
Luridiana, V., Peimbert, A., Peimbert, M., & Cerviño, M. 2003, ApJ, 592, 846
Mas-Hesse, J. M., & Kunth, D. 1991, A&AS, 88, 399
Mouhcine, M., Lewis, I., Jones, B., et al. 2005, MNRAS, 362, 1143
Moustakas, J., Kennicutt, R. C., & Tremonti, A. 2006, ApJ, 642, 775
Olofsson, K. 1989, A&AS, 80, 317
Pagel, B. E. J., Edmunds, M. G., Blackwell, D. E., Chun, M. S., & Smith, G. 1979, MNRAS, 189, 95
Peimbert, M., Peimbert, A., & Ruiz, M. T. 2000, ApJ, 541, 688
Pilyugin, L. S., Thuan, T. X., & Vílchez, J. M. 2003, A&A, 397, 487
Rosa-González, D., Terlevich, E., & Terlevich, R. 2002, MNRAS, 332, 283
Salpeter, E. E. 1955, ApJ, 121, 161
Schaerer, D., & de Koter A. 1997, A&A, 322, 598
Schaerer, D., Charbonnel, C., Meynet, G., Maeder, A., & Schaller, G. 1993a, A&AS, 102, 339
Schaerer, D., Meynet, G., Maeder, A., & Schaller, G. 1993b, A&AS, 98, 523
Schaller, G., Schaerer, D., Meynet, G., & Maeder, A. 1992, A&AS, 96, 269
Schmutz, W., Leitherer, C., & Gruenwald, R. 1992, PASP, 104, 1164
Stasińska, G. 2004, in Cosmochemistry. The melting pot of the elements. XIII Canary Islands Winter School of Astrophysics, ed. C. Esteban, & R. J. García López, A. Herrero, & F. Sánchez (Cambridge: Cambridge Univ. Press), 115
Stasińska, G. 2007, in The Emission-Line Universe, ed. J. Cepa, & F. Sanchez (Cambridge: Cambridge Univ. Press), in press [arXiv:0704.0348]
Stasińska, G., & Izotov, Y. 2003, A&A, 397, 71
Stasińska, G., & Leitherer, C. 1996, ApJS, 107, 661
Stasińska, G., Schaerer, D., & Leitherer, C. 2001, A&A, 370, 1
Veilleux, S., & Osterbrock, D. E. 1987, ApJS, 63, 295
Vílchez, J. M., & Esteban, C. 1996, MNRAS, 280, 720
Vílchez, J. M., & Pagel, B. E. J. 1988, MNRAS, 231, 257
Villaverde, M., Cerviño, M., & Luridiana, V. 2009, in prep.
White, S. D. M., & Audouze, J. 1983, MNRAS, 203, 603
Wilmes, M., & Koeppen, J. 1995, A&A, 294, 47
van Zee, L., Salzer, J. J., Haynes, M. P., O'Donoghue, A. A., & Balonek, T. J. 1998, AJ, 116, 2805
Zurita, A., Beckman, J. E., Rozas, M., & Ryder, S. 2002, A&A, 386,801